Urban Climate 69 (2026) 103103

Contents lists available at ScienceDirect

Urban Climate

journal homepage: www.elsevier.com/locate/uclim

Urban climate evaluation in the upcoming generation of CMIP6-Driven EURO-CORDEX regional climate simulations☆

Javier Diez-Sierra [a,*], Natalia Zazulie [b,c,d], Gaby S. Langendijk [e], Yaiza Quintana [a], Marianna Adinolfi [f], May Bohmann [g], Lars Buntemeyer [h], Erasmo Buonomo [i], Steven Caluwaerts [j,k], Angelo Campanale [f], Rita M. Cardoso [l], David Carvalho [m], Ana Casanueva [n,o], Matthias Demuzere [p], Theodore Endreny [q], Jesús Fernández [a], Nicolas Ghilain [k,r], Klaus Goergen [s], Tomas Halenka [t], Peter Hoffmann [h], Eleni Katragkou [u], Sven Kotlarski [v,w], Patrick Ludwig [g], Vera Maurer [x], Josipa Milovac [a], Rita Nogherotto [y,b], Vasileios Pavlidis [u], Joni-Pekka Pietikäinen [h], Mario Raffa [f], Diana Rechid [h], Jan-Peter Schulz [x,f], Fien Serras [z], Andres Simon-Moral [a,aa], Pedro M.M. Soares [l], Stefan Sobolowski [ab], Claas Teichmann [h], Kobe Vandelanotte [j,k], Inne Vanderkelen [k,z], Fuxing Wang [ac]

[a] Instituto de Física de Cantabria (IFCA), CSIC-Universidad de Cantabria, Santander, Spain
[b] The Abdus Salam International Centre for Theoretical Physics (ICTP), Trieste, Italy
[c] Istituto Nazionale di Geofisica e Vulcanologia,Sezione Roma 2, Roma, Italy
[d] Department of Atmospheric and Ocean Sciences, Faculty of Exact and Natural Sciences, University of Buenos Aires (DCAO-FCEN-UBA) - National Council of Scientific and Technical Research (CONICET), Buenos Aires, Argentina
[e] Climate Adaptation and Disaster Risk Department, Deltares, Delft, the Netherlands
[f] CMCC Foundation - Euro-Mediterranean Center on Climate Change, Italy
[g] Institute of Meteorology and Climate Research – Troposphere Research (IMKTRO), Karlsruhe Institute of Technology (KIT), Karlsruhe, Germany
[h] Climate Service Center Germany (GERICS), Helmholtz-Zentrum Hereon, Fischertwiete 1, 20095 Hamburg, Germany.
[i] Met Office, Hadley Centre, Exeter, UK
[j] Department of Physics and Astronomy, Ghent University, Belgium
[k] Royal Meteorological Institute of Belgium, Brussels, Belgium
[l] Instituto Dom Luiz, Faculdade de Ciências, Universidade de Lisboa, 1749-016 Lisboa, Portugal
[m] CESAM - Physics Department, Aveiro University, Aveiro, Portugal
[n] Departamento de Matemática Aplicada y Ciencias de la Computación, Universidad de Cantabria, Santander, Spain
[o] Grupo de Meteorología y Computación, Unidad Asociada al CSIC, Santander, Spain

☆ This article is part of a Special issue entitled: 'Climate Change and Cities' published in Urban Climate.

* Corresponding author.

E-mail addresses: javier.diez@unican.es (J. Diez-Sierra), nzazulie@ictp.it (N. Zazulie), quintanay@unican.es (Y. Quintana), marianna.adinolfi@cmcc.it (M. Adinolfi), rnoghero@ictp.it (M. Bohmann), lars.buntemeyer@hereon.de (L. Buntemeyer), erasmo.buonomo@metoffice.gov.uk (E. Buonomo), steven.caluwaerts@ugent.be (S. Caluwaerts), angelo.campanale@cmcc.it (A. Campanale), rmcardoso@ciencias.ulisboa.pt (R.M. Cardoso), david.carvalho@ua.pt (D. Carvalho), ana.casanueva@unican.es (A. Casanueva), matthias@b-kode.be (M. Demuzere), te@esf.edu (T. Endreny), jesus.fernandez@ifca.unican.es (J. Fernández), nicolas.ghilain@meteo.be (N. Ghilain), k.goergen@fz-juelich.de (K. Goergen), tomas.halenka@mff.cuni.cz (T. Halenka), peter.hoffmann@hereon.de (P. Hoffmann), katragou@geo.auth.gr (E. Katragkou), sven.kotlarski@meteoswiss.ch (S. Kotlarski), patrick.ludwig@kit.edu (P. Ludwig), vera.maurer@dwd.de (V. Maurer), milovacj@unican.es (J. Milovac), vapavlid@physics.auth.gr (V. Pavlidis), joni-pekka.pietikaeinen@hereon.de (J.-P. Pietikäinen), mario.raffa@cmcc.it (M. Raffa), diana.rechid@hereon.de (D. Rechid), janpeter.schulz@cmcc.it (J.-P. Schulz), fien.serras@kuleuven.be (F. Serras), andres.simon@tecnalia.com (A. Simon-Moral), pmsoares@ciencias.ulisboa.pt (P.M.M. Soares), stefan.p.sobolowski@uib.no (S. Sobolowski), claas.teichmann@hereon.de (C. Teichmann), kobe.vandelanotte@meteo.be (K. Vandelanotte), inne.vanderkelen@kuleuven.be (I. Vanderkelen), fuxing.wang@smhi.se (F. Wang).

https://doi.org/10.1016/j.uclim.2026.103103
Received 30 March 2026; Received in revised form 31 July 2026; Accepted 14 August 2026
Available online 31 August 2026

[p] B-Kode VOF, Ghent, Belgium
[q] Department of Environmental Resources Engineering, State University of New York College of Environmental Science and Forestry (SUNY ESF), Syracuse, NY, USA
[r] Department of Geography, Liège University, Belgium.
[s] Institute of Bio- and Geosciences (Agrosphere, IBG-3), Forschungszentrum Jülich, Jülich, Germany
[t] Charles University, Faculty of Mathematics and Physics, Department of Atmospheric Physics, Prague, Czechia
[u] Department of Meteorology and Climatology, School of Geology, Aristotle University of Thessaloniki, Greece
[v] Federal Office of Meteorology and Climatology MeteoSwiss, Operation Center 1, CH-8058, Zurich-Airport, Switzerland
[w] Center for Climate Systems Modeling C2SM, ETH, Zurich, Zurich, Switzerland
[x] Deutscher Wetterdienst, Offenbach am Main, Germany
[y] The Institute of Atmospheric Sciences and Climate (CNR-ISAC), Bologna, Italy
[z] Department of Earth and Environmental Science, KU Leuven, Leuven, Belgium
[aa] TECNALIA, Basque Research and Technology Alliance (BRTA), Derio, Spain
[ab] Geophysical Institute, University of Bergen and Bjerknes Centre for Climate Research, Bergen, Norway
[ac] Swedish Meteorological and Hydrological Institute, Folkborgsvägen 17, 60176 Norrköping, Sweden

ARTICLE INFO

Keywords:
Urban climate
regional climate model
CORDEX
CMIP6
urban-rural contrast
urban parameterization

ABSTRACT

The latest EURO-CORDEX simulations, downscaling CMIP6 GCMs, provide an improved representation of urban areas compared to the previous CORDEX-CMIP5 generation, partly motivated by the increasing demand for urban-scale climate information for adaptation and planning, as reflected in the IPCC Special Report on Climate Change and Cities.

In this study, we evaluate the ERA5-driven EURO-CORDEX ensemble (CMIP6 generation) for its ability to represent urban areas and simulate urban climate across nearly 100 European cities. We further assess the sensitivity of urban–rural contrasts to geographical location and urban parameterization schemes. Results show that the urban heat island effect is captured in most cities, with a more realistic representation in models that include urban canopy schemes. The urban dry island effect and wind speed attenuation are also identified, although they exhibit greater inter-model variability than temperature.

Models identify spatial patterns across the analyzed cities, including geographical climatic gradients, the urban cool island effect in arid regions, and coastal influences. Comparison with observations highlights challenges in evaluating RCMs, underscoring the need for dense and representative observational networks or alternative approaches.

This work provides the first systematic evaluation of urban climate representation in EURO-CORDEX, identifies suitable sub-ensembles, and informs future model development.

1. Introduction

Cities are highly vulnerable to climate change due to their high population density, extensive land surface modification, and concentration of infrastructure and economic activities (IPCC, 2023; UN-Habitat, 2015). In Europe, where more than 75% of the population lives in urban areas ("World Bank.,", n.d.), climate change and urbanization interact to amplify heat-related risks, posing growing challenges for public health, infrastructure, and energy systems.

Urban areas modify the local climate primarily through changes in the surface energy balance, reduced evapotranspiration, increased heat storage in built materials, altered surface roughness, and anthropogenic heat emissions (Dong et al., 2017; Masson et al., 2020; Oke et al., 2017). These processes give rise to the Urban Heat Island (UHI) effect, whereby urban areas are warmer than their rural surroundings, particularly during nighttime. The combined effect of the UHI and global warming can raise urban temperatures dramatically, increasing the risk of heat wave–related mortality in cities under future scenarios (Huang et al., 2026; Klimiuk et al., 2025; Lemonsu et al., 2023; Nogueira and Soares, 2019; Schäfer et al., 2025). Beyond temperature, urban areas can influence other climatic variables. For instance, precipitation may increase over and downwind of highly urbanized areas (Burian and Shepherd, 2005; Doan et al., 2022; Han et al., 2014; Liu and Niyogi, 2019; Shepherd, 2006), while relative humidity is often lower in urban zones compared to rural surroundings (Holmer and Eliasson, 1999; Kuttler et al., 2007; Langendijk et al., 2019; Zhao et al., 2021), and wind patterns can be markedly altered within cities (Baidar et al., 2020; Childs and Raman, 2005; Droste et al., 2018; Lee, 1979). Moreover, urbanization alters urban air quality increasing concentrations of key air pollutants such as $PM_{2.5}$ and O_3 and their associated health risks (Zhan et al., 2023). As climate change raises background temperatures, understanding the two-way interactions between urban areas and the regional climate has become increasingly important in order to develop effective adaptation strategies. This growing importance is reflected in the preparation of the IPCC Special Report on Climate Change and Cities within the Seventh Assessment Report (AR7) cycle.

The Coordinated Regional Climate Downscaling Experiment (CORDEX) provides a common framework for coordinated high-resolution regional climate projections worldwide (Giorgi Jr, 2015; Gutowski Jr. et al., 2016a,b). CORDEX simulations constitute an important line of evidence in IPCC assessments and underpin numerous regional climate services and impact assessments (Diez-Sierra et al., 2022; Gutiérrez et al., 2021; Iturbide et al., 2022). Regional Climate Models (RCMs) can investigate interactions between cities and the regional climate over decadal timescales (Hamdi et al., 2020; Langendijk et al., 2024). Recent advances towards kilometer-scale simulations have improved the representation of mesoscale processes and land–atmosphere interactions, while convection-permitting RCMs enable explicit representation of deep convection (Coppola et al., 2020; Garbero et al., 2021; Hundhausen et al., 2023; Langendijk et al., 2022; 2021; Lucas-Picher et al., 2021; Prein et al., 2015; Schär et al., 2020). While many urban climate studies have focused on individual cities or limited ensembles (Argüeso et al., 2016; Krayenhoff et al., 2018; Kusaka et al., 2012; Langendijk et al., 2022; 2021a,b; Michau et al., 2025), the CORDEX Flagship Pilot Study on Urban Environments and Regional Climate Change (FPS URB-RCC) has extended these analyses towards coordinated high-resolution ensemble simulations for urban areas (Langendijk et al., 2024). Importantly, the high computational cost of convection-permitting simulations limits their applicability for global climate model ensemble studies (Pedruzo-Bagazgoitia et al., 2026), making coordinated regional climate simulations such as CORDEX an essential source of climate information for urban areas.

Within the previous CMIP5 generation of CORDEX simulations, several studies assessed the representation of urban areas and their climatic impacts. Langendijk et al. (2026) evaluated the representation of 1,741 cities in the CORDEX-CORE ensemble at the 25 km and 12.5 km spatial resolution and demonstrated that increasing spatial resolution and implementing more sophisticated urban parameterizations improved the simulation of the UHI, despite persistent underestimation of urban extent. The study employed a consistent and reproducible methodology originally developed by Diez-Sierra et al. (2025) to delineate urban and rural areas. The methodology is implemented in the urban layer of the Copernicus Interactive Climate (C3S) Atlas (https://atlas.climate.copernicus.eu), an evolution of the IPCC WGI Interactive Atlas (https://interactive-atlas.ipcc.ch), which provides climate change projections for a subset of the cities analyzed in this study. Subsequently, Zazulie et al. (2026) analyzed climate hazards across 40 European and North African cities using the EURO-CORDEX CMIP5 ensemble at 12.5 km resolution, demonstrating robust increases in heat-related hazards under future warming while highlighting the persistence of urban–rural contrasts.

The new generation of EURO-CORDEX simulations driven by CMIP6 (CORDEX-CMIP6; Katragkou et al., 2024; Sobolowski et al., 2025) provides several important advances over the previous CMIP5 generation. These include a broader implementation of physically based Urban Canopy Models (UCMs), improved urban fraction and land-use/land-cover datasets, and, in selected model configurations, the inclusion of prescribed historical and future land-cover changes and interactive vegetation coupling. Together, these developments are expected to improve the representation of urban processes and their two-way interactions with the regional climate.

Despite these advances, a systematic evaluation of urban climate representation in the ERA5-driven EURO-CORDEX CMIP6 ensemble has not yet been performed. Therefore, this study addresses this gap by providing the first coordinated evaluation of urban climate representation in the ERA5-driven EURO-CORDEX CMIP6 ensemble across 93 major European cities. Specifically, we assess (i) how realistically the new generation of CMIP6 driven regional climate models represents urban areas, and (ii) how well they reproduce observed urban imprints in near-surface air temperature, relative humidity, and wind speed. The results provide the evaluation basis for future urban climate projections within EURO-CORDEX, continues the work carried out by the FPS URB-RCC for the previous generation of CORDEX-CMIP5 models, and will contribute to further development of the urban layer of the Copernicus Climate Change Service (C3S) Interactive Climate Atlas.

2. EURO-CORDEX-CMIP6 experiment design

Katragkou et al. (2024) and Fernandez et al. (2026) described the protocol for a CMIP6-driven EURO-CORDEX RCM simulation ensemble and its overall evaluation, respectively. As noted in these works, the only focus domain in this model generation is the higher-resolution EUR-12 domain, with ~12,5 km grid spacing (denoted "EUR-11" in the previous generation). Model diversity has increased, particularly due to different variants of some models exploring different levels of complexity. From a user's perspective, this means that the grand ensemble cannot be used in a purely probabilistic way; additional considerations are necessary, as many simulations are interdependent.

In this section, we focus on describing differences between RCMs in terms of their urban representation describing those simulations which are fit for this purpose (*urban ensemble*). We recommend consulting the overall evaluation paper for a comprehensive overview of the EURO-CORDEX-CMIP6 *grand ensemble* (Fernandez et al., 2026). A full model description table is found in EURO-CORDEX (2023). Table 1 summarizes the main characteristics of the RCMs considered in this study, focusing on their land-surface and urban representations. A key aspect highlighted in Table 1 is the substantial heterogeneity in the land-cover input used across models, both in terms of the underlying dataset and the reference period they represent. Land-cover periods differ significantly among RCMs, ranging from fixed historical snapshots (e.g. around the 1990's or early 2000's) to more recent (e.g. 2015) or even annually evolving land-cover representations. Within CORDEX FPS LUCAS, high resolution Plant Functional Type (PFT) maps based on ESA CCI (European Space Agency Climate Change Initiative) land cover data including urban areas (LANDMATE PFT) have been developed for 1992-2015 by Reinhart et al. (2022). The urban representation in LANDMATE PFT has been found suitable for its use in RCMs and shows added value regarding the accuracy of the spatial location of urban areas (Reinhart et al., 2021). This dataset for 2015 is used by several RCMs contributing to this study. Land use/land cover (LULC) differences may span more than a decade between models and can therefore have a considerable impact on the models representation of urban areas. As a consequence, the extent, intensity, and spatial distribution of urban surfaces, and thus the simulated urban imprint, may vary substantially across models, independently of the urban scheme itself. This heterogeneity needs to be taken into account when interpreting inter-model differences in urban climate signals and related diagnostics.

In the RCMs ensemble considered, two distinct groups (or sub-ensembles) can be identified based on their urban parameterizations. RCMs with a bulk approach (hereafter referred to as bulk models) conceptualize urban areas in a simplified way, representing cities as a single homogeneous surface, typically impervious or "rock" surfaces, with averaged properties such as albedo, heat capacity, and roughness. In contrast, RCMs with UCMs (hereafter referred to as UCM models) provide a single- or multi-layer urban canopy

Table 1
Urban characteristics and model-specific urban components in the EURO-CORDEX-CMIP6 ensemble. The table includes the RCM name and version, the responsible institute, the land-surface model (LSM), the urban scheme (if any), the type of urban representation (e.g. bulk or UCM), the type of surface tile (sfturf) used to represent urban areas (dominant or fractional), the land-cover dataset employed, and the reference period of the land-cover data. Some models only provide the evaluation (ev) simulation. Rows in italics indicate EURO-CORDEX models not considered in this study, either because they were not available at the time of the analyses, they are very similar to other model configurations included, or they do not represent any urban area (see text).

RCM Name and version	RCM Version	Institute	Land model name	Urban scheme type	Urban scheme name	Type of urban fraction (sfturf)	Land cover input	Land cover (period)
ALARO1-SFX	v1-r1	RMIB-UGent	SURFEX	UCM (single layer)	TEB	fraction	ECOCLIMAP-I	1990
CNRM-ALADIN64E1	v1-r1	CNRM-MF	SURFEX	bulk (treated by the vegetation model ISBA as rocks, without any modified parameters)	NA	Fraction (the town fraction is converted to “nature” and treated by the vegetation model ISBA as rocks)	ECOCLIMAP-I	1990
HCLIM43-ALADIN	v1-r1	SMHI	SURFEX	UCM (single layer)	TEB	fraction	ECOCLIMAP-SG (Second Generation)	2010
CCLM6-0-1	v1-r1	CLMcom-Hereon	TERRA	bulk	NA	fraction	GLC2000	2000
CCLM6-0-1-URB	v1-r1	CMCC	TERRA	bulk	TERRA_URB	fraction	GLC2000	2000
CCLM6-0-1-URB-ESG (ev)	v1-r1	CLMcom-KUL	TERRA	bulk	TERRA_URB	fraction	ECOCLIMAP-Second Generation	2018/2019
TSMP1-140E (COSMO, CLM, ParFlow)	v1-r1	CLMcom-FZJ	CLM v3.5	None (urban areas are treated as bare soil)	NA	NA	GLC2000	2000
CCLM5-0-9-NEMOMED12-3-6	v1-r1	CLMcom-GUF	TERRA	None	NA	NA	GlobCover 2009	2009
ICON-CLM-202407-1-1	v1-r1	CLMcom-Hereon	TERRA	bulk	TERRA_URB	fraction	GLOBCOVER v2.3	2009
ROAM-NBS	v1-r1	DWD-BSH	TERRA	bulk	TERRA_URB	fraction	GLOBCOVER v2.3	2009
RegCM5-0	v1-r1	ICTP	CLM4.5	UCM (single layer)	CLMU	fraction	MODIS	2005
REMO2020-2-2	v1-r1	GERICS	REMO2020 LULC: GLCC V2, Rechid et al., 2008	bulk	NA	Fraction available, but model used only land fraction and urban influenced its characteristics	GLCC V2	1992/1993
REMO2020-2-2-MR2 (ev)	*v1-r1*	*GERICS*	*REMO2020 LULC: GLCC V2,* Rechid et al., 2008	*bulk*	*NA*	*Fraction available, but model used only land fraction and urban influenced its characteristics*	*GLCC V2*	*1992/1993*
REMO2020-2-2-iMOVE	v1-r1	GERICS	REMO2020-iMOVE (interactive MOsaic based VEgetation): Wilhelm et al., 2014 REMO land surface scheme described in Pietikäinen et al. (2025)	bulk	NA	Fraction available, but model used only land fraction and urban influenced its characteristics	LANDMATE PFTs (Reinhart et al., 2022)	2015

(*continued on next page*)

Table 1 (*continued*)

RCM Name and version	RCM Version	Institute	Land model name	Urban scheme type	Urban scheme name	Type of urban fraction (sfturf)	Land cover input	Land cover (period)
REMO2020-2-2-iMOVE-LUC	*v1-r1*	*GERICS*	*REMO2020-iMOVE (interactive MOsaic based VEgetation):*Wilhelm et al., 2014*, REMO land surface scheme described in*Pietikäinen et al. *(2025)*	*bulk*	*NA*	*Fraction available, but model used only land fraction and urban influenced its characteristics*	*LANDMATE PFTs /LUCAS LUC (* Hoffmann et al., *2023)*	*1979-2020 (annual prescribed maps)*
REMO2020-2-2-TEB (ev)	v1-r1	GERICS	REMO2020 LULC: GLCC V2, Rechid et al., 2008	UCM (single layer)	TEB	fraction	ECOCLIMAP-SG (GLCC V2)	2015 for urban fraction (1992/1993for the rest)
WRF451Q	v1-r1	IDL	Noah-MP	bulk	NA	dominant	LANDMATE PFT (Reinhart et al., 2022)	2015
WRF451Q	*v1-r2*	*CESAM*	*Noah-MP*	*bulk*	*NA*	*dominant*	*LANDMATE PFT (* Reinhart et al., 2022*)*	*2015*
WRF451Q	*v1-r3*	*AUTH*	*Noah-MP*	*bulk*	*NA*	*dominant*	*LANDMATE PFT (* Reinhart et al., 2022*)*	*2015*
RACMO23E	v1-r1	KNMI	HTESSEL	bulk	NA	fraction	LANDMATE PFT (Reinhart et al., 2022)	2015
HadREM3-GA7-05	v1-r1	UKMO	Jules	bulk	NA	fraction	ESA CCI v1.6.1	2010

description of cities, simplifying urban geometry, commonly through idealized infinite street canyons and focusing on the surface energy budget. Depending on their level of complexity, some UCMs distinguish between components such as roofs, walls, roads, and trees, while others adopt more aggregated representations. UCMs allow for a more realistic simulation of urban energy budgets and microclimates including also the effect of anthropogenic heat sources such as building heating in winter, air conditioning in summer, and vehicle traffic.

The UCM sub-ensemble includes four models: ALARO1-SFX, HCLIM43-ALADIN, RegCM5-0 and REMO2020-2-2-TEB (see Table 1). GCOAST-AHOI2-1 would also belong to this group; however, its simulations were not available at the time of the analyses and were therefore not included in this study. RegCM5-0 uses the Community Land Model version 4.5 (CLM4.5) as its land-surface scheme (Oleson et al., 2013a, 2013b). Urban areas are simulated using the CLM Urban (CLMU) single-layer urban canopy model (SLUCM), where the urban fraction is divided into three density classes, tall building district, high density, and medium density, and represented by canyon surfaces (roofs, sunlit and shaded walls, and pervious and impervious ground). The scheme also accounts for building energy processes through prescribed indoor temperatures, allowing anthropogenic waste heat from space heating and air conditioning to be optionally included in the urban energy budget (Oleson et al., 2013a, 2013b). REMO2020-2-2-TEB, HCLIM43-ALADIN, and ALARO1-SFX all represent urban surfaces using the physically-based single-layer Town Energy Balance (TEB) urban canopy model (Masson, 2000) coupled with its force-restore Building Energy Model (BEM) (Bueno et al., 2012; Masson et al., 2002). In each configuration, TEB describes the urban environment using an idealized infinite street-canyon geometry and resolves separate surface energy budgets for roofs, walls, roads, and urban vegetation. In REMO2020-2-2-TEB, the atmosphere–surface interaction is handled by REMO's own land-surface model (Pietikäinen et al., 2025; Rechid et al., 2008), while the TEB module is based on the SURFEX v9.0 implementation (Pietikäinen et al., 2025) and urban fractions are derived from the ECOCLIMAP-SG dataset (Stewart and Oke, 2012). In HCLIM43-ALADIN and ALARO1-SFX, the land-surface component is provided by SURFEX (versions v8.1 and v8.0, respectively), with urban areas in both systems represented using the TEB+BEM scheme.

The bulk sub-ensemble comprises the remaining models, including those unavailable at the time of the study. Within this sub-ensemble, REMO2020-2-2-MR2 shares the same urban configuration as REMO2020-2-2 but differs in its use of the MERRA-2 aerosol climatology (Pietikäinen et al., 2025). As it does not introduce any changes in urban representation, it was excluded from the analysis. REMO2020-2-2-iMOVE corresponds to REMO2020-2-2 coupled interactively to MOsaic based VEgetation (iMOVE, Wilhelm et al., 2014), using the new LULC dataset LANDMATE (Reinhart et al., 2022), while REMO2020-2-2-iMOVE-LUC further incorporates LULC changes for the past and for the future according to the corresponding Shared Socioeconomic Pathway SSP (Hoffmann et al., 2023). These new datasets and model configurations were developed within the CORDEX FPS on Land Use and Climate Across Scales (LUCAS; Rechid et al., 2017). For consistency with the other models, in which land use and urban fractions are prescribed and time-invariant, REMO2020-2-2-iMOVE-LUC was excluded from the present analysis. However, this simulation is the only RCM in the ensemble that represents evolving urban areas, which constitutes a significant improvement for evaluating the urban imprint in both historical simulations and future projections. Of particular relevance, REMO2020-2-2-TEB uses the same model configuration as REMO2020-2-2 but replaces the bulk approach with an UCM, enabling a direct assessment of the added value of the UCM within the same modelling framework. COSMO-CLM (CCLM) has been shown to be able to represent urban dynamics over some cities, with improvements relative to the ERA5 reanalysis (Adinolfi et al., 2023) and is included here in two configurations: CCLM6-0-1-URB and CCLM6-0-1-URB-ESG, differing in their land surface forcing data sets. CCLM6-0-1-URB adopts a fine-resolution dataset for the Impervious Surface Area (ISA), arising from the European Environment Agency (EEA) imperviousness / soil-sealing product (Maucha et al., 2010) and GLC2000 as land-cover dataset, while CCLM6-0-1-URB-ESG uses ECOCLIMAP-SG as land-cover map, which also provides local climate zones. Therefore, both simulations represent different urban areas and should be treated as different members of the ensemble. The basic configuration of CCLM6-0-1 and CCLM6-0-1-URB is exactly the same, based on Russo et al. (2024) and Geyer et al. (2026), however CCLM6-0-1-URB and CCLM6-0-1-URB-ESG feature the TERRA_URB parametrization (Wouters et al., 2016; 2015). This bulk urban land-surface scheme represents the variability of ground heat and moisture transport, the turbulent transfer of momentum, heat and moisture, and the surface–atmosphere radiative exchanges in urban areas. TERRA_URB has been extensively evaluated in previous studies (Trusilova et al., 2016; Wouters et al., 2016; 2015), demonstrating skill in reproducing the different urban surface energy balance components and the UHI. ICON-CLM-202407-1-1 includes the same TERRA_URB urban parameterization (Campanale et al., 2025; Schulz and Vogel, 2020) and an updated version (GLC2009) of the land-cover dataset used in CCLM6-0-1-URB (GLC2000). In ICON-CLM-202407-1-1, the urban fraction was originally smoothed by default to reduce the urban effect at higher resolutions (~3 km) in the CPRCM configuration to avoid a nighttime summer warm bias and this smoothed urban fraction is also used in the EUR-12 simulations considered here. Only one WRF451Q realization (v1-r1) is included in the analysis, as all of the three available share the same model configuration, with the only difference of being run on different computers. They are based on the Noah-MP land surface model (Niu et al., 2011) in which urban areas are defined via the LANDMATE PFT LULC (Reinhart et al., 2022), as in REMO, but WRF urban categories use a binary (0 and 1) dominant cover representation. Finally, HadREM3-GA7-05 is identical to that used in the previous generation (CORDEX-CMIP5) which was also nested into ERA-Interim (Tucker et al., 2022). It uses a land-cover dataset from the ESA Land Cover CCI project team ("Dataset Record: ESA Land Cover Climate Change Initiative (Land_Cover_cci): Global Land Cover Maps, Version 1.6.1," n.d.) and the JULES (Best et al., 2011) land surface scheme which includes tiles for all land types in each grid cell. The urban component is estimated by treating the urban part as the canopy (Best, 2005). This simulation provides a reference to assess the impact of changing the driving reanalysis from ERA-Interim to ERA5.

Several RCMs were not available at the time of this evaluation: CCLM6-0-1, TSMP1-140E, CCLM5-0-9-NEMOMED12-3-6, GCOAST-AHOI1-1, GCOAST-AHOI2-1 and WRF451Q_v1-r3. In addition, GCOAST-AHOIB1-1 (r1-v1 and r1-v2) does not include any urban

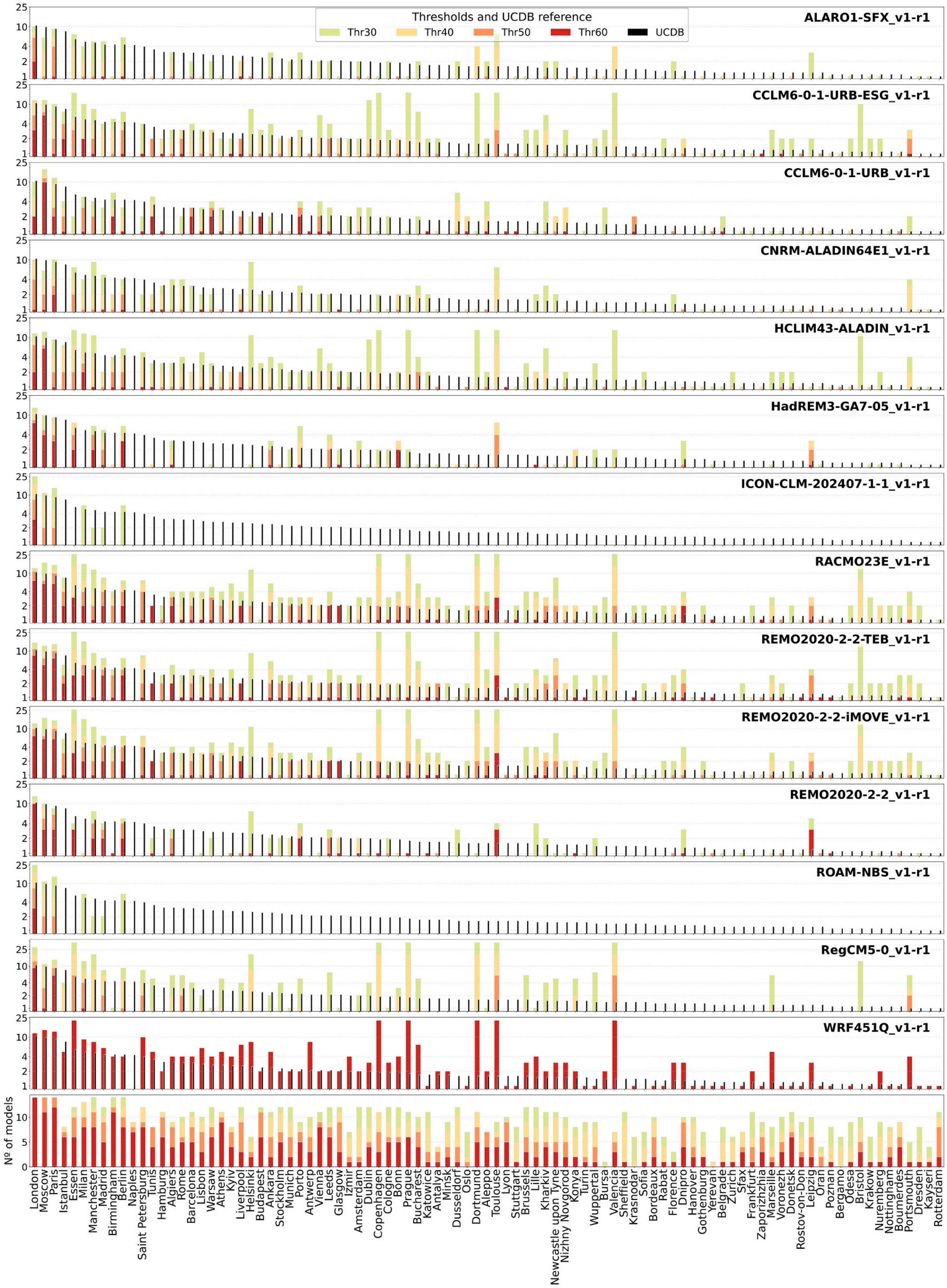

(caption on next page)

Fig. 1. Number of grid cells classified as urban for different urban fraction thresholds (30%, 40%, 50%, 60%) across the ERA5-driven EURO-CORDEX models (rows) and cities. The bottom row shows the number of models (out of 14) containing at least one urban grid cell for each threshold and city (cities are sorted by decreasing number of models meeting this criterion). Black bars represent the number of urban grid cells derived from the GHS-UCDB dataset (version R2024A) within the urban core. Only those cities represented by at least one urban grid cell in at least one RCM were included in the analysis.

parameterization or representation and is therefore unable to show any urban effect. GCOAST-AHOI2-1 is very similar to ICON-CLM-202407-1-1 and ROAM-NBS in terms of their urban representation, as they share the atmospheric and land surface components, including the TERRA_URB model.

3. Methods

Cities were selected using the GHS-UCDB ("Global Human Settlement - Urban Centre database R2024A - European Commission," n.d.), considering only urban centres larger than the grid spacing of the EURO-CORDEX simulations (12.5 km). The urban fraction from each RCM was then used to assess city representation and the spatial extent of urban areas. Urban and rural areas were subsequently delineated using the model-consistent algorithm of Diez-Sierra et al. (2025), which relies on urban fraction, land fraction, and orography. Using these urban–rural delineations, urban–rural contrasts were calculated for monthly means of four near-surface climate variables: daily minimum and maximum near-surface air temperatures (tasmin and tasmax), wind speed (sfcWind) and relative humidity (hurs). The urban–rural contrasts of tasmin and tasmax are used here as proxies for nocturnal and diurnal UHI intensities. It should be noted that these contrasts may occur at different times of the day between urban and rural areas. UHI intensity refers specifically to the atmospheric urban heat island, not the surface-UHI, based on skin temperature. Urban–rural contrast is used more broadly across all analyzed variables, while urban imprint refers to the full suite of urban-induced climatic modifications represented by the models in urban areas. The analyzed period is 1991–2020, which is covered by the protocol for evaluation simulations over the EURO-CORDEX domain (Katragkou et al., 2024). Results were first assessed in 14 cities with observational data and then extended to the full set of 93 cities, with a focus on the differences between the UCM and bulk sub-ensembles, geographical location (coastal, inland, mountainous), and IPCC AR6 regions.

3.1. City selection

Cities were selected based on a minimum urban area of 156 km^2, which approximately corresponds to the horizontal grid spacing of the EURO-CORDEX ensemble (12.5 x 12.5 km), within the EURO-CORDEX domain (Nikulin et al., 2025). Following Diez-Sierra et al. (2025) and Langendijk et al. (2026), the GHS-UCDB dataset (version R2024A) was used as a reference to compare the spatial extent of cities represented in the RCMs, as it provides information on the geometry and area of "urban centers" worldwide (Melchiorri et al., 2024). This database offers a globally consistent and harmonized representation of urban centres as polygons derived from population and built-up area criteria, using data from the Global Human Settlement Layer (GHSL) combined with other open datasets, making it a suitable reference for evaluating the urban extent simulated by the RCMs. Note that, in the GHS-UCDB dataset, urban centres represent only the core built-up area and therefore have a substantially smaller spatial extent than the corresponding administrative city boundaries. As a result, the criterion applied for city selection is based on the characteristics of the urban core rather than the full administrative area; therefore, several European cities were excluded even though their full administrative boundaries are larger than 156 km^2 (e.g. Zagreb, Bremen, Volgograd and Belfast).

A total of 95 cities were selected based on the latter criterion (shown in Table 1SM in the Supplementary Materials) and included in the analysis. The cities are grouped according to their geographical location (coastal, inland and mountainous) and the IPCC AR6 regions (Iturbide et al., 2020), also indicated in Table 1SM. Coastal cities are defined as urban cores located within one grid cell (12.5 km) of the coastline, while mountain cities are defined as those situated at elevations above 500 m.

3.2. Urban and rural delineation

To delineate urban areas and their corresponding rural surroundings within RCM outputs, we employ the algorithm developed by Diez-Sierra et al. (2025), which has been previously used in recent studies (Langendijk et al., 2026; Zazulie et al., 2026). The algorithm relies on three static model variables: urban fraction (sfturf), land area fraction (sftlf), and orography (orog), thereby ensuring that the delineation reflects urban land cover and topography from each model. Urban grid cells are identified using a minimum urban fraction threshold; in this study, we used a threshold of 40% after performing a sensitivity analysis (see Section 4.1). Rural surroundings are selected from neighboring grid cells that satisfy a set of constraints: urban fraction lower than 5%, sufficient land coverage (land area fraction larger than 70%), and similar elevation to urban cells, defined using a threshold equal to the maximum elevation difference within the urban cells or 100, whichever is higher). Subsequently, a morphological dilation process is applied iteratively to expand the rural mask outward from the urban core until a target rural-to-urban grid-cell ratio is reached (2 in this study). For the WRF451Q model, the treatment differs slightly, as the urban fraction is provided as a binary mask (urban = 1, non-urban = 0) rather than a continuous fraction variable. Consequently, the 40% and 5% thresholds cannot be applied directly but are instead interpreted in accordance with this categorical definition.

This strategy enables a consistent yet adaptable classification of urban and rural areas across different cities and RCMs, and has been validated across multiple CORDEX domains (Diez-Sierra et al., 2025; Langendijk et al., 2026). In contrast to methods based purely on coordinate- or GIS-based approaches (Guerreiro et al., 2018; Schwingshackl et al., 2024; Smid et al., 2019), the methodology proposed by Diez-Sierra et al. (2025) explicitly incorporates RCM-specific urban representations and results in a more robust, model-aware delineation of urban and rural environments which ensures methodological consistency across the multi-model and multi-city analysis.

4. Results

4.1. Representation of urban areas

The number of grid cells classified as urban varies considerably across EURO-CORDEX models and cities for different urban fraction thresholds (30%, 40%, 50%, 60%), as shown in Fig. 1, where black bars indicate the GHS-UCDB reference values. The bottom panel shows the number of models that identify at least one urban grid cell for every city and for all of tested urban fraction thresholds. The results reveal a pronounced heterogeneity in the representation of urban areas across models. Some models capture most European cities with urban fractions above 40%, including HCLIM43-ALADIN (70 cities), REMO2020-2-2-TEB (84), RACMO23E (80), and WRF451Q (86). In contrast, others, such as ICON-CLM-202407-1-1 and ROAM-NBS, identify only four cities each, which are the largest metropolitan areas of London, Moscow, Paris, and Milan. These four major cities are consistently identified by all models at urban fraction thresholds above 40%. The higher number of urban grid cells detected by REMO2020-2-2-TEB compared to REMO2020-2-2 partly reflects the more recent land-cover dataset used in the TEB configuration, ECOCLIMAP-SG (2015) instead of GLCC V2 (1992/1993) (Pietikäinen et al., 2026), highlighting the sensitivity of urban representation to differences in land-cover time period. Notably, REMO2020-2-2-iMOVE, which is based on the LANDMATE land-cover dataset for 2015, shows a similar increase in urban grid-cell detection and leads to conclusions that are fully consistent with those derived from REMO2020-2-2-TEB.

In WRF451Q, the dominant type of urban fraction (see Table 1) means that an urban fraction of 100% is assigned to a grid cell if the urban category dominates the other land use categories within the same grid cell (otherwise it is set to 0%). Note that this can happen with urban fractions below 50%, which results in higher urban areas when compared with the other models (Fig. 1). Furthermore, the smoothing applied to the urban fraction in the ICON configuration (ICON-CLM-202407-1-1; see Section 2) may be overly restrictive at the coarser 12 km CORDEX resolution. While this approach can be beneficial at convection-permitting scales, it leads to a dilution of the urban signal. As a result, urban land-use effects are underrepresented, which explains the lower frequency of urban detection in ICON-based models (including ROAM-NBS) compared to CCLM6-0-1-URB and CCLM6-0-1-URB-ESG, where the same urban scheme is applied without such smoothing.

The results of the sensitivity analysis of the urban threshold (see Fig. 1 and Fig.s 7SM–9SM) indicate that a 40% threshold is appropriate for defining cities at the EURO-CORDEX grid spacing, consistent with previous studies conducted at the same resolution (Diez-Sierra et al., 2025; Langendijk et al., 2026; Zazulie et al., 2026). As shown in Fig.s 7SM–9SM, the choice of the urban fraction threshold influences the estimated UHI intensities. However, its impact is generally limited, with only a few city–RCM combinations showing noticeable differences. Furthermore, adopting higher urban fraction thresholds (e.g., 60%) substantially reduces the number of cities available for analysis. Even though 95 cities fulfilled the initial requirement related to the urban core, two of them (i.e. Roquetas de Mar in Spain and Erbil in Iraq) had to be excluded as they were not represented by any RCM with at least one urban grid cell with the 40% urban fraction threshold. This results in a total of 93 cities for the subsequent analysis.

As illustrated in Fig. 1, several models detect a larger number of cities when thresholds below 40% are applied. However, in these cases the spatial extent of cities in the RCMs tends to be overestimated relative to the GHS-UCDB dataset. It should be noted that, while this study uses the GHS-UCDB 2024 version as a reference, each RCM relies on land-cover data from different periods (see Table 1). This inconsistency may influence the comparison of urban extents across models and should be taken into account when interpreting the results.

Additionally, the urban areas of some cities, such as Manchester and Liverpool in England, and Düsseldorf and Wuppertal in Germany, are overestimated in all models as they are joined by grid cells with urban fractions exceeding 40%. As a result, their urban areas cannot be analyzed independently and must instead be treated as a single urban conglomerate. Fig. 1SM illustrates the Manchester and Liverpool case, and together with Fig. 1, highlights the challenges of performing a consistent and fair inter-model comparison, given the substantial heterogeneity in urban area representation across models.

4.2. Urban-rural contrast

Urban–rural contrasts, defined here as differences in climate variables between urban areas and their rural surroundings, were analyzed for the 93 selected cities over the period 1991–2020 and for the monthly means of the four near-surface variables defined in Section 3: tasmin, tasmax, sfcWind, and hurs. UHI intensity refers specifically to temperature-based urban–rural contrasts, as defined in Section 3.

Fig. 2 illustrates the methodology used to calculate the urban–rural contrast for the four climate variables analyzed in this study, based on the urban–rural masks derived from each EURO-CORDEX model (see Section 3.2). The fig. presents an example for Paris, showing the nocturnal (tasmin) UHI intensity over the period 1991–2020 for four RCMs with different treatments of urban areas: CCLM6-0-1-URB, REMO2020-2-2-TEB, REMO2020-2-2, and WRF451Q. Fig. 2SM in the Supplementary Materials shows the results for the complete ensemble, including both nocturnal (tasmin) and diurnal (tasmax) UHI intensities.

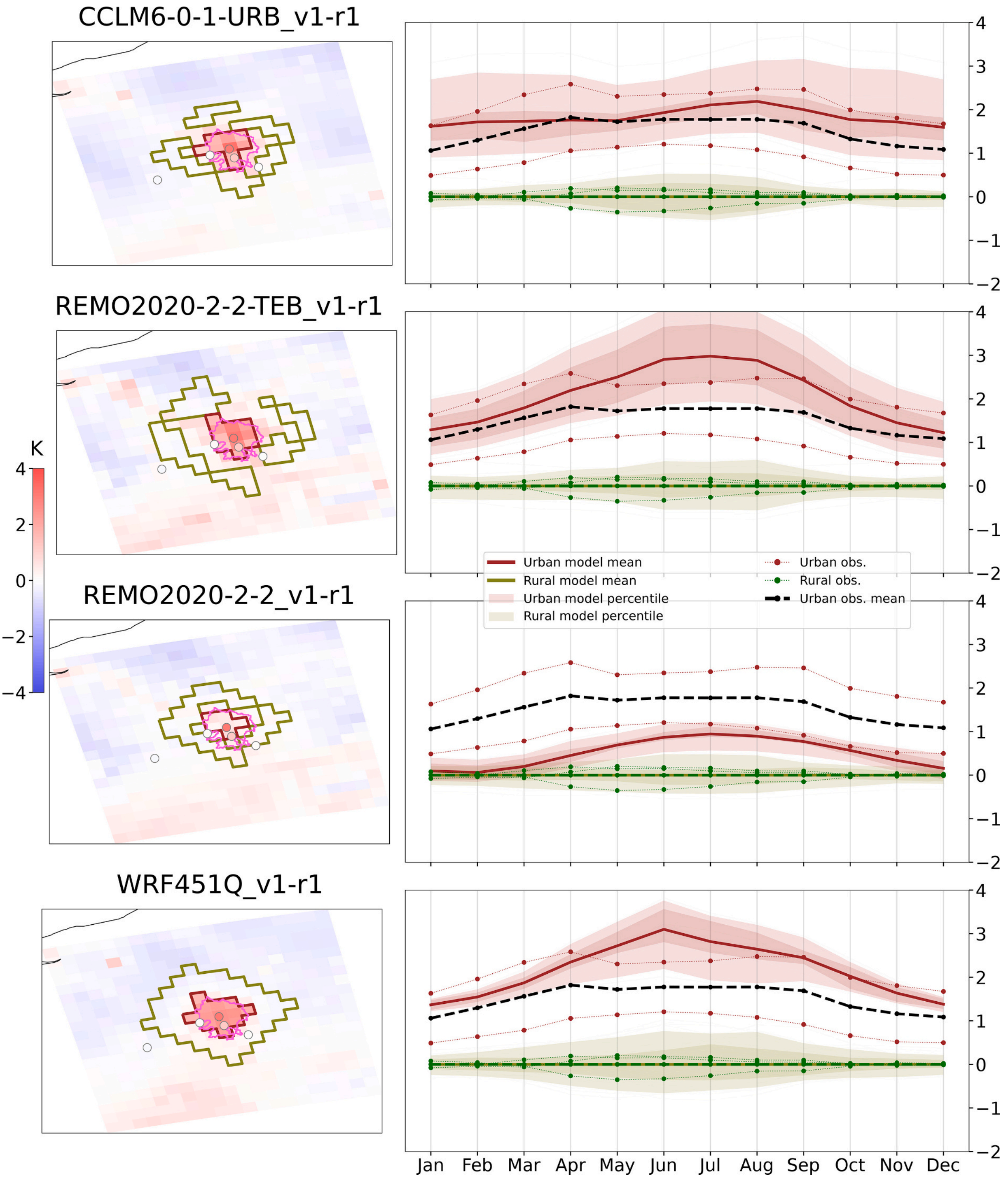

Fig. 2. Minimum temperature anomalies comparing urban areas (maroon polygons) with their surrounding rural areas (olive-green polygons) for Paris across four different RCMs (rows). The spatial maps (left panels) display the urban–rural contrast annual climatology, obtained by subtracting the mean rural climatology (i.e. spatial mean of all grid cells within the olive green polygon) from the climatology at each grid point. Annual cycles (right panels) are computed for each urban (maroon polygon) and rural (olive green) grid cell relative to the mean rural climatology for every month. The mean and selected percentiles (5, 25, 75, 95) of the urban–rural UHI are shown for the annual cycles. Météo-France observational data at individual stations are included for reference on the maps and as time series (dotted red and green lines indicate urban and rural stations, respectively, and the black dashed line indicates the mean observed UHI intensity).

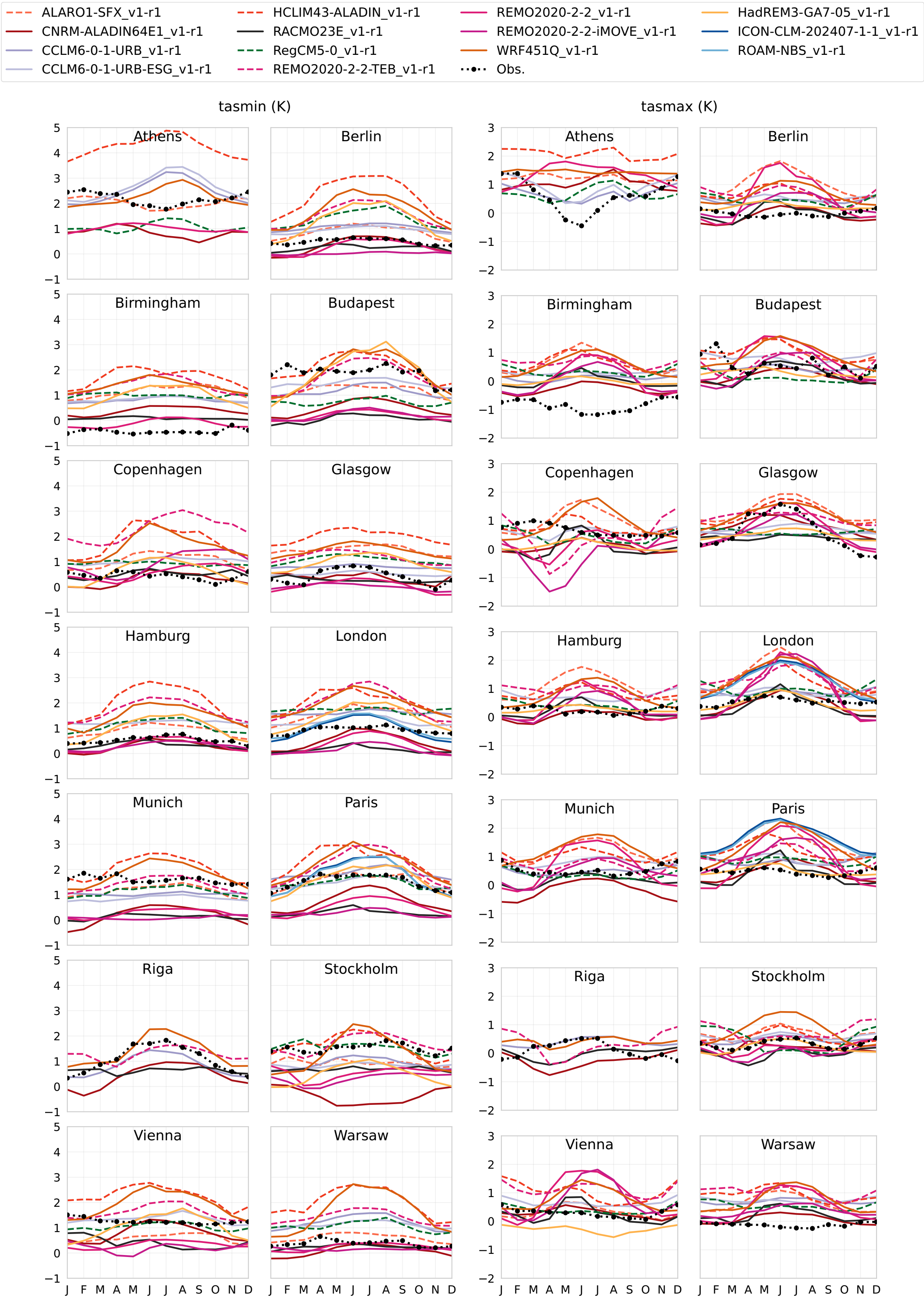

(caption on next page)

Fig. 3. Annual cycle anomalies between urban areas and their surroundings for minimum (left) and maximum (right) temperatures for 14 cities in the EURO-CORDEX domain. For observational data (GHCNd, ECA&D, and Météo-France for Paris), the urban vs. rural classification follows GHS-UCDB urban center polygons. Panels display the average UHI intensity for both UCM RCMs (dashed lines) and bulk RCMs (solid lines), and observations (black dotted lines).

Analysis of urban area representation and UHI intensity for Paris (Fig.s 2 and 2SM), benchmarked against five Météo-France observation sites (black lines), reveals considerable heterogeneity among RCMs relative to the GHS-UCDB database. The stations PARIS-MONTSOURIS and ORLY are classified as urban, while CHARTRES, MELUN, and TOUSSUS-LE-NOBLE are classified as rural. Fig. 2 shows a clear improvement for the UCM models: REMO2020-2-2-TEB follows more closely the observations as compared to the simple bulk approach of REMO2020-2-2. Similarly, CCLM6-0-1-URB, which uses a bulk approach, but integrates the TERRA_URB scheme, reproduces the annual observed values accurately. Finally, the WRF451Q model, based on a bulk approach with a dominant urban fraction, performs reasonably well in reproducing nocturnal UHI intensity, although it tends to substantially overestimate diurnal UHI intensities (see Fig. 2SM). It is important to note that the land-cover datasets correspond to different time periods among RCMs, which complicates direct comparison and evaluation against observations. These results further emphasize that spatial aggregation hides the variability of UHI intensity across the city, a limitation well documented by observational studies showing strong intra-city differences associated with local urban morphology and land-cover characteristics (Arnds et al., 2017; Lehnert et al., 2025; Roth et al., 2022).

4.2.1. Evaluation

To assess the capability of the RCMs to represent the urban-rural contrast effect, we use daily observational data from the Global Historical Climatology Network (GHCNd; Menne et al., 2012) and the European Climate Assessment and Dataset (ECA&D; Klein Tank et al., 2002), as they constitute two of the most comprehensive in situ observational datasets over Europe. ECA&D provides a particularly dense station network derived from national meteorological services, enabling robust characterization of spatial temperature variability, although station density varies regionally (Hofstra et al., 2009). For Paris, the analysis was performed using five Météo-France stations (see Section 4.2. above). Stations were classified as urban or rural based on the GHS-UCDB polygons representing the urban cores of each city, except in the case of Paris, where the precise location of stations is known and the ones located in large urban parks were excluded, as they do not exhibit typical urban characteristics. Those located within the urban polygon were considered urban, while stations outside but within the surrounding area were designated as rural. To maintain consistency, elevation differences were taken into account: rural stations exceeding the elevation threshold defined for each city and RCM were excluded (see Section 3.2). Finally, to ensure a robust representation, stations were required to provide at least ten non-consecutive years, each with at least 95% daily data coverage. In total, fourteen cities met the selection criteria (see Fig.s 3 and 4), each with at least one urban and one rural station. We relied on these extended datasets to cover as many cities as possible. Ideally, carefully selected station data sampling the urban and surrounding areas for each of the cities should be employed for evaluation. Unfortunately, such a dataset is not available. To partially overcome this limitation, we extensively compare our results with those of other studies carried out for individual cities using curated datasets.

Following Langendijk et al. (2026), observational data were used as a qualitative benchmark rather than for direct quantitative comparison, since point measurements cannot be directly compared with model grid-cell averages. In addition, many urban stations are typically located in green or open areas (e.g. airports), which may lead to an underestimation of the UHI intensity (Peterson, 2003) and should therefore be considered when interpreting the results. Of the 14 cities selected based on data availability, London, Riga, Birmingham, Athens, Glasgow, and Warsaw have only 2 or 3 stations each, which makes the results highly dependent on the locations of these stations. In London and Birmingham, the urban stations (1 and 2, respectively) are located outside the edge of the city center, in low-density urban areas; in Athens, two of the three stations are situated very close to the coast. In cities with multiple observations located both within and outside urban areas, such as Berlin, Budapest, Hamburg, Stockholm, and Vienna, the estimated urban–rural contrast is likely attenuated, as it is derived from spatial averages, and different land use classes. A visual inspection of stations locations shows that, some of the rural stations are located in villages or airports, which may dampen the rural signal, while most of the urban stations are located in low-density suburban neighbourhoods, which may reduce the observed urban signal.

The annual cycles of temperature differences between urban and rural areas for the 14 European cities with available observational data are shown in Fig. 3. The results indicate that the observed UHI intensities for most cities fall within the range of the EURO-CORDEX ensemble for both minimum and maximum temperatures, except for specific cases such as Birmingham (for tasmin and tasmax) and Athens (for tasmax), where the RCMs show a different seasonal pattern. RCMs generally overestimate the seasonal amplitude of UHI intensity relative to observations, with differences between UCM and bulk models. For diurnal (tasmax) UHI, the annual cycle is less pronounced in several UCM models, which in some cases simulate higher UHI intensities in winter than in summer (particularly REMO2020-2-2-TEB and RegCM5-0). In contrast, bulk models generally exhibit stronger UHI in summer, with the exception of ROAM-NBS, RACMO23E, CCLM6-0-1-URB and CCLM6-0-1-URB-ESG. UCM models generally simulate higher nocturnal (tasmin) UHI intensities. Despite not being a UCM, the WRF451Q bulk configuration also produces high nocturnal values due to its treatment of urban fractions based on a dominant land-cover approach.

Although the general behaviour is consistent across most cities, some notable differences emerge when individual locations are compared with previous studies. The observed UHI intensities for the 14 cities are generally weaker than those reported in the literature, likely reflecting the station network limitations discussed above. Among the analysed cities, Athens exhibits the largest UHI intensities throughout the year, particularly for nocturnal (tasmin) UHI, with lower values during the summer months for both

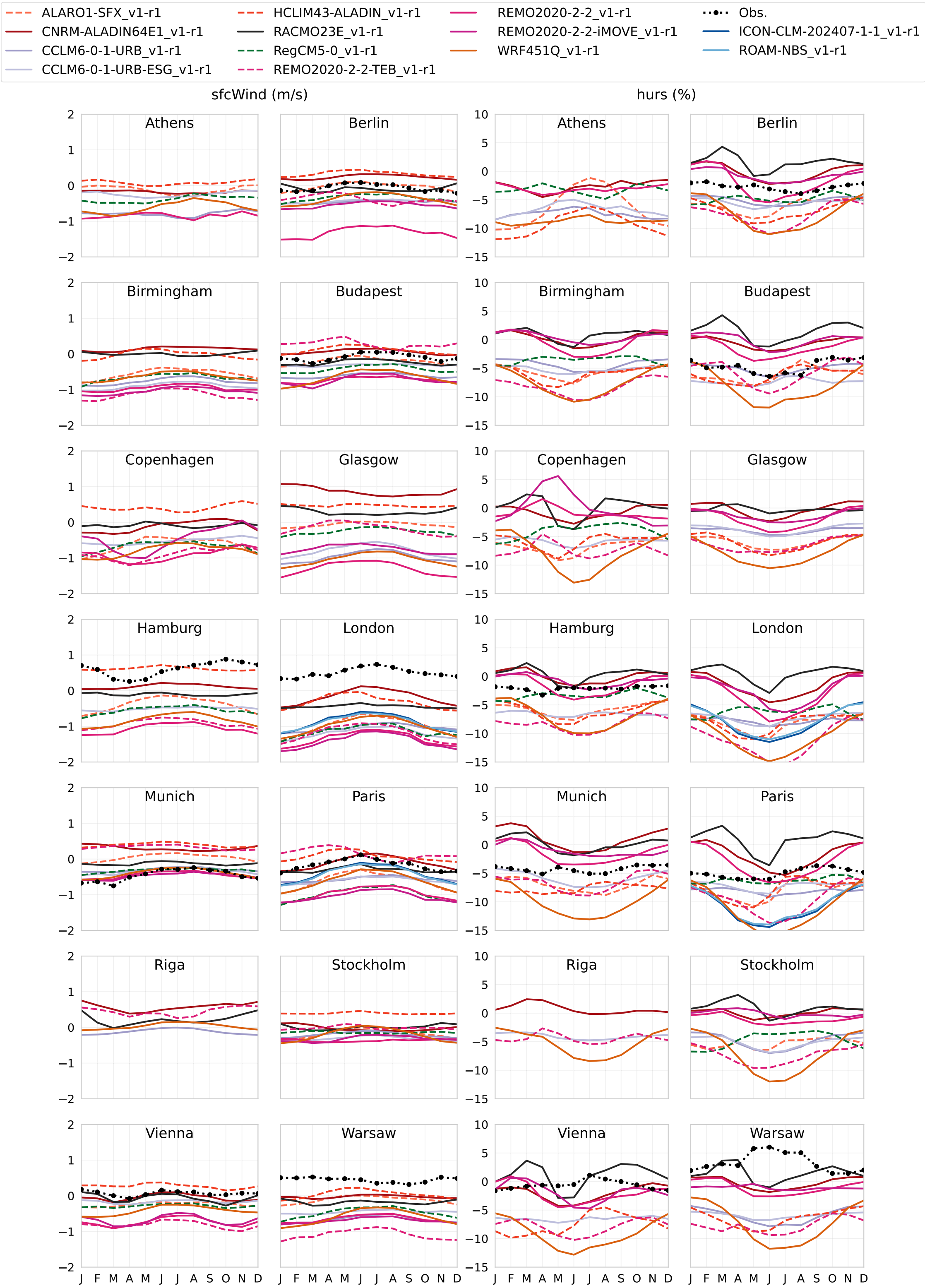

Fig. 4. Same as Fig. 3 but for near-surface wind speed (sfcWind; m/s) and near-surface relative humidity (hurs; %).

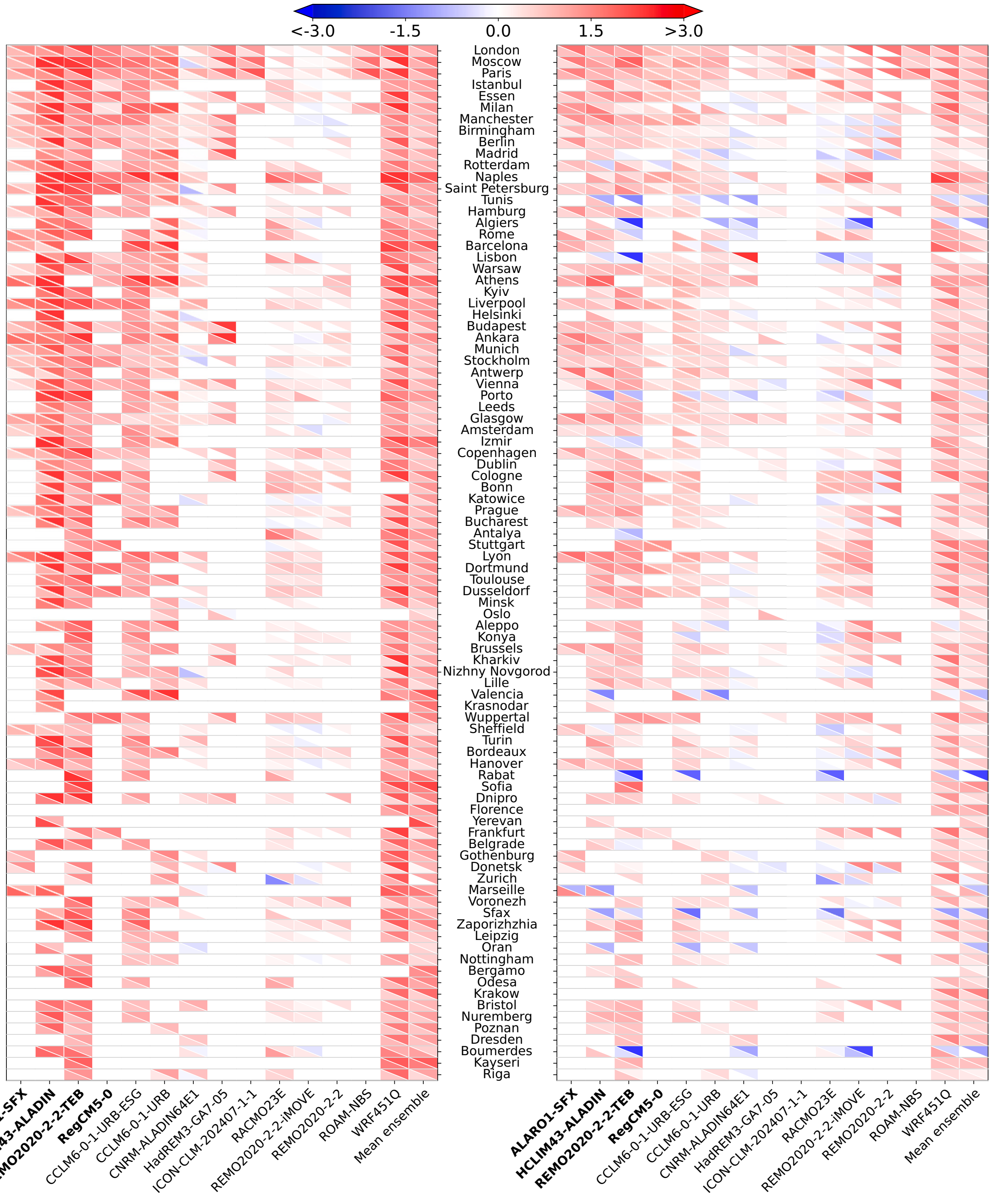

Fig. 5. Heat map of the UHI intensity [K] for JJA (upper triangles) and DJF (lower triangles) across all EURO-CORDEX domain cities (rows) and RCMs (those with a UCM are shown in bold in the x axis). Minimum temperatures are shown in the left panels, and maximum temperatures in the right panels. Cities are sorted by decreasing urban center extension according to the GHS-UCDB dataset. The last column for each panel corresponds to the ensemble mean results. Fig.s 3SM and 4SM in the Supplementary Material present the urban–rural contrast values for each city and each RCM.

variables. This contrasts with the literature, which generally reports larger values and an opposite seasonal cycle (Founda et al., 2015; Founda and Santamouris, 2017). The annual cycle simulated by the RCMs exhibits a large spread, especially for nocturnal (tasmin) UHI, with most models exhibiting maximum intensities during the summer months, more consistent with the literature.

Across the remaining cities, RCMs generally simulate a stronger seasonal amplitude and higher summertime UHI intensities than the observations. For several cities, including Berlin, Hamburg, Birmingham, Warsaw, Stockholm, Paris, and (for nocturnal UHI)

London, the seasonal cycle simulated by the RCMs is more consistent with previous studies than with the observations used here (Fenner et al., 2014 for Berlin; Schlünzen et al., 2010 for Hamburg; Zhang et al., 2014 for Birmingham; Kuchcik et al., 2024 for Warsaw; Le Roy et al., 2020; Michau et al., 2022 for Paris and Wilby, 2003 for London). Conversely, Budapest and the diurnal UHI in London and Paris show better agreement between the observations used here and the literature (Pongracz et al., 2010 for Budapest; Le Roy et al., 2020 and Michau et al., 2022 for Paris and Wilby, 2003 for London). Munich represents an exception, with relatively weak seasonality reproduced by some RCMs, although considerably inter-model spread remains. A detailed city-by-city comparison between the urban–rural contrast simulated by the RCMs and the available literature is provided in the SM.

The differences between UCM and bulk models, to reproduce nocturnal (tasmin) UHI intensities, can be interpreted through their representation of urban energy balance processes. UCMs explicitly resolve urban canyon geometry, including longwave radiation trapping and reduced sky-view factors, which enhance nighttime heat retention, and some, but not all, represent anthropogenic heat fluxes, including waste heat from building space conditioning, which can amplify UHI intensity. In contrast, the simplified homogeneous rock surfaces in bulk models have lower effective thermal storage and more efficient nocturnal radiative cooling, leading to a more rapid dissipation of heat accumulated during the daytime (Langendijk et al., 2026). During the day, UCM models also account for the trapping of shortwave radiation within urban canyons. Fig. 2SM for Paris shows that several bulk models fail to capture the observed nocturnal UHI intensity (specially REMO2020-2-2, RACMO23E and CNRM-ALADIN64E1). Similar behaviour was already identified in the previous EURO-CORDEX generation (Langendijk et al., 2019; Zazulie et al., 2026), where the earlier versions of these models (REMO2015, RACMO22E and CNRM-ALADIN63) systematically underestimated nocturnal UHI intensity across many cities. More generally, when comparing the two EURO-CORDEX generations, models available in both ensembles (here and in Zazulie et al., 2026) tend to exhibit a broadly similar seasonal behaviour of the UHI signal. This, together with the strong seasonality exhibited by bulk models, which tend to overestimate diurnal (tasmax) UHI in summer compared with observations, suggests that UCM models may perform better.

The urban-rural contrasts for near-surface wind speed (sfcWind) and near-surface relative humidity (hurs) are shown in Fig. 4. The analysis of sfcWind reveals no consistent urban-rural contrast in observations across cities, with minimal seasonality. In contrast, for hurs, most cities exhibit an Urban Dry Island (UDI) effect in the observations (i.e., a reduction in moisture availability in urban areas relative to surrounding rural sites), with the exception of Warsaw. Overall, the available observational data for both variables are very limited, and sfcWind does not reveal a consistent signal, highlighting the need for alternative reference datasets to evaluate urban climate in RCMs.

Several studies generally report a decrease in wind speed due to the presence of buildings and other obstacles (Chen et al., 2021; Mikhailuta et al., 2017). However, this reduction is not spatially uniform, as some studies report locally increased wind speeds of up to 40% (Mikhailuta et al., 2017). In contrast, other urban areas may experience up to 300% more frequent calm periods than surrounding rural sites, suggesting that urban wind conditions are overall more variable and less predictable (Chen et al., 2021). Additionally, under certain atmospheric conditions higher wind speeds and turbulence were observed at the downwind site over the entire urban boundary layer outside the urban canopy layer (Baidar et al., 2020). In the present study, observations do not reveal a clear pattern for near-surface wind speed, highlighting the strong influence of station locations. For example, rural stations around Warsaw are located in villages or near forests, while the only urban station is located at the airport, resulting in higher near-surface wind speeds in the urban area than at the rural stations. In contrast, most RCMs indicate a reduction in wind speed in urban areas compared with surrounding rural sites, consistent with the literature.

For near-surface relative humidity, UDI effect is evident in most RCMs. UCM models tend to simulate larger reductions. However, similar behaviour is also found in WRF451Q, CCLM6-0-1-URB, and the ESG version, which are not UCM configurations. In contrast, bulk models exhibit stronger seasonality. It is important to note that relative humidity depends strongly on temperature; therefore, the generally higher UHI intensities simulated by UCM models are consistent with a stronger UDI effect. The stronger UDI effect in summer simulated by bulk models may result from an overestimation of the diurnal UHI effect during this season. For several cities, such as Berlin, London, and Paris, the UCM models capture the stronger UDI effect in spring, as reported in the literature (Huang and Song, 2023; Langendijk et al., 2022). For Athens, ALARO1-SFX and HCLIM43-ALADIN exhibit seasonal patterns that differ from the rest of the ensemble, with greater reductions in relative humidity in urban areas during the winter months. Observational UDI results show a weaker UDI effect compared with the UCM models.

The literature generally reports the presence of a UDI in most cities, attributed to increases in near-surface air temperatures and to changes in moisture availability associated with the expansion of impervious surfaces, which reduce infiltration and soil water availability for evapotranspiration (Meili et al., 2022). However, the specific configuration of urban or rural weather station sites can strongly affect the identification and magnitude of the UDI (Siu and Hart, 2013). Huang and Song (2023) provide an extensive review for 34 cities, including Vienna (UDI between −1 and −6%), Berlin (UDI between −2 and −10%), Munich (UDI between −4 and −7%) and London (UDI between −3 and −7%). Their results indicate that mid-latitude cities generally exhibit moderate UDI effects, while cities with low annual precipitation and pronounced dry and wet seasons may experience more extreme UDI effects. UDI intensities are strongest in spring, and coastal locations tend to exhibit weaker signals due to sea-breeze moisture transport. Overall, the literature on near-surface relative humidity suggests that the UDI signal may be attenuated in the observational data used in this study, and that UCM models provide a more realistic representation than the bulk schemes.

REMO2020-2-2 and REMO2020-2-2-TEB allow for an evaluation of the added value of the UCM approach compared to the bulk one within this RCM. For nocturnal UHI intensity (tasmin, Fig. 3), the UCM exhibits higher urban–rural contrasts across all cities, consistent with the literature. For diurnal UHI (tasmax, Fig. 3), the bulk model shows a more pronounced seasonal cycle, with peak intensities in summer, whereas the UCM simulates a smoother variation, with several cities experiencing stronger UHI in winter, in agreement with literature. Near-surface wind speed (sfcWind, Fig. 4) generally decreases more in the UCM model across most cities, except in Birmingham, Copenhagen, Hamburg, and London, where both configurations show similar reductions; in Warsaw, however,

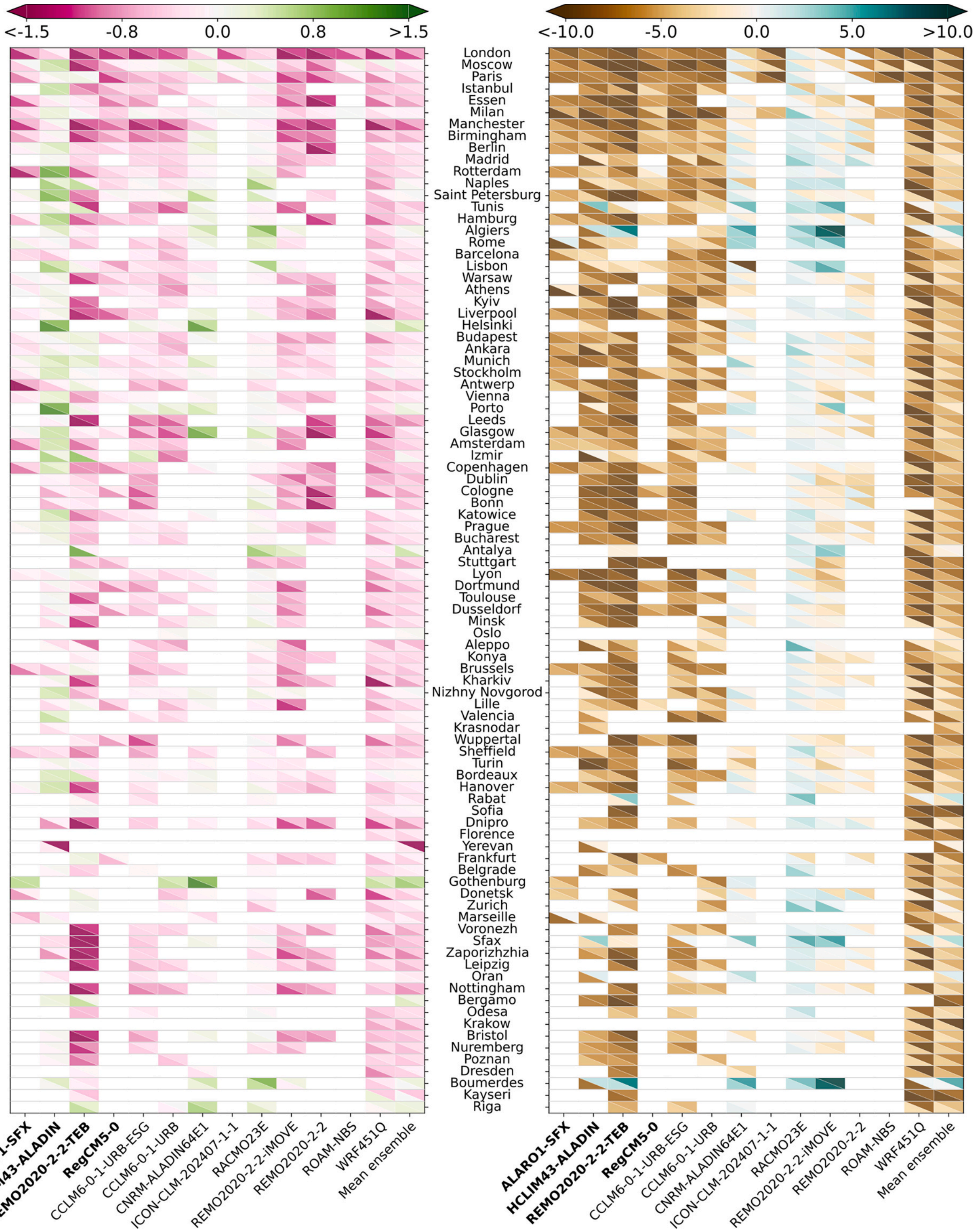

Fig. 6. Same as Fig. 5 but for near-surface wind speed (sfcWind; m/s) and near-surface relative humidity (hurs; %). Fig.s 5SM and 6SM in the Supplementary Material present the urban–rural contrast values for each city and each RCM.

the bulk model exhibits a larger decrease. For near-surface relative humidity (hurs, Fig. 4), the UDI effect is more intense in the UCM, with values close to those reported in the literature for Vienna, Berlin, Munich, and London.

4.2.2. Model intercomparison

The analysis, initially conducted for the 14 cities with observational data, was extended to the full set of 93 cities considering only model results (no observations). To summarize the findings, in this section we focus on seasonal mean contrasts between urban and rural areas for summer (JJA) and winter (DJF).

Heat maps of UHI intensities across the 93 selected cities within the EUR-12 domain (rows) and RCMs (columns) (Fig. 5) reveal significant inter-model variation in intensity, though the urban–rural contrast signal is generally consistent across cities. In the case of nocturnal UHI (left panel), the two sub-ensembles of models are clearly distinct. UCM models show higher nocturnal UHI intensities. However, similar behaviour is also found in WRF451Q, CCLM6-0-1-URB, and the ESG version, which are not UCM configurations. HCLIM43-ALADIN shows, in general, the highest nocturnal UHI intensities. Several bulk models, such as REMO2020-2-2, RACMO23E,

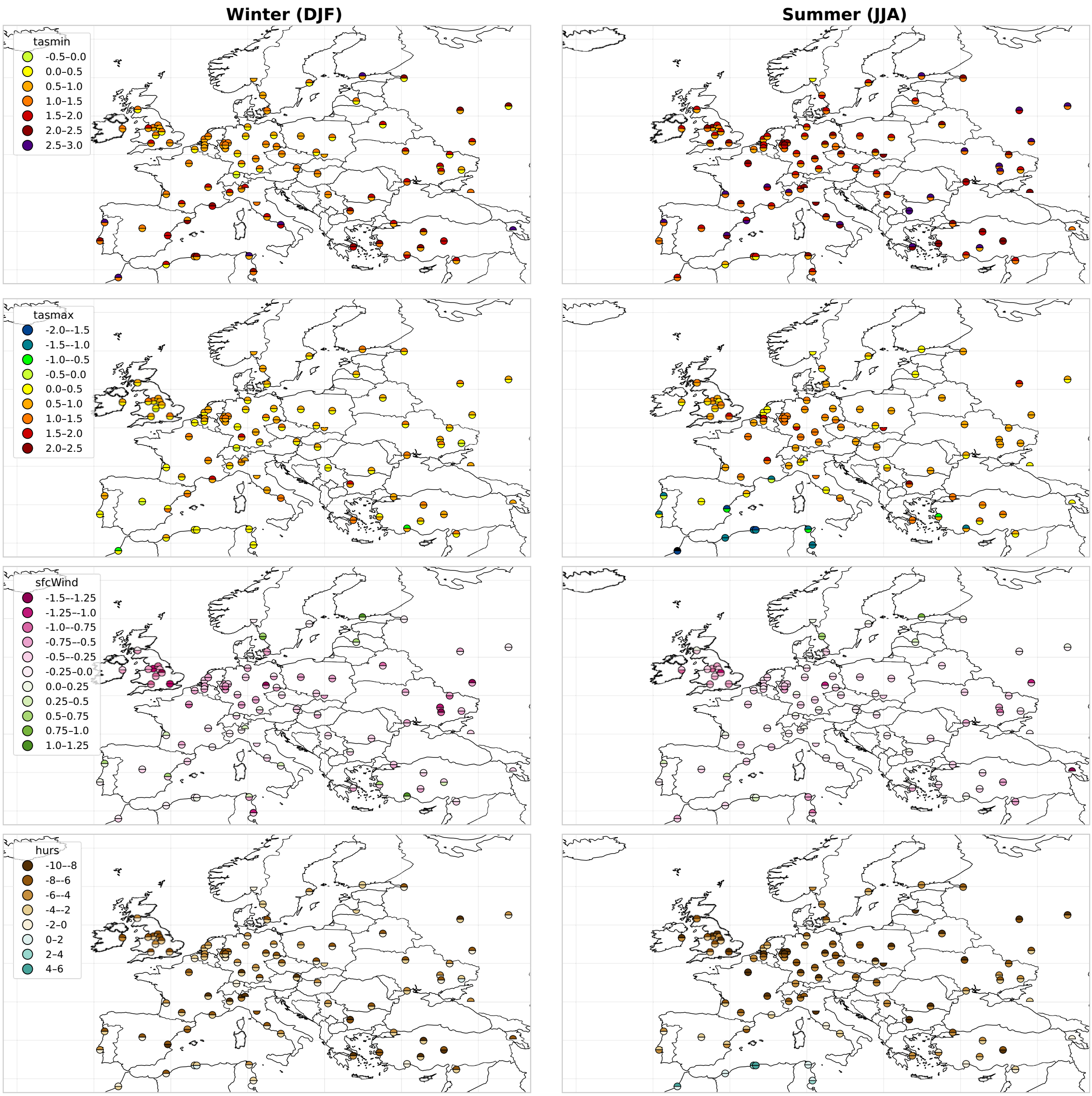

Fig. 7. Urban-rural contrasts for minimum and maximum near-surface temperatures (tasmin and tasmax; K), near-surface wind speed (sfcWind; m/s), and near-surface relative humidity (hurs; %) during winter (DJF, left) and summer (JJA, right). Each dot represents the multi-model ensemble mean for each European city. The upper and lower middle circle represent the UCM (n = 4) and the bulk (n = 10) sub-ensembles, respectively.

or CNRM-ALADIN64E1, exhibit values close to 0 or even negative values during the winter months. For diurnal UHI intensity (right panel), the differences between the two sub-ensembles are less pronounced. Several models show negative values during the summer months, for both sub-ensembles. This behaviour is particularly evident in several North African cities (e. g. Tunis, Algiers, Rabat, Sfax, Oran and Bourmerdes), where negative daytime values in maximum temperature suggest the occurrence of an urban cool island effect during summer. Such effects have been documented in arid and semi-arid environments, where surrounding areas can become warmer than urban areas during the day due to the sparse vegetation cover and strong surface heating, while urban materials and shading may limit daytime temperatures (Lazzarini et al., 2013; Rasul et al., 2016; Yang et al., 2017). Detectable negative values of the diurnal UHI (right panel) intensities can also be observed in several coastal cities with hot summers, such as Marseille, Porto, Lisbon, Izmir, Antalya and Valencia. In these cases, the proximity of urban areas to the sea may act as a climatic moderator, mitigating urban temperatures relative to surrounding rural areas. This phenomenon is attributed to the higher thermal inertia of the ocean and the influence of sea breezes, which tend to reduce heat accumulation in the city during daytime hours (Nogueira et al., 2020). Comparing the ensemble mean results (last columns) for both variables (tasmin and tasmax), we observe that UHI intensity is higher at night, especially during summer, a result that is well documented in the literature (Hamdi et al., 2020; Karlický et al., 2018; Masson et al., 2020; Nogueira et al., 2022; WMO, 2023).

Analogous heat maps for near-surface wind speed (sfcWind) and near-surface relative humidity (hurs) (Fig. 6) show that most models simulate reductions within urban areas relative to surrounding rural regions for both variables. For near-surface wind, the effect is generally more pronounced during winter. Three models (HCLIM43-ALADIN, CNRM-ALADIN64E1, and RACMO23E) exhibit distinct patterns, showing positive urban–rural contrast values for several cities. REMO2020-2-2-TEB displays the largest reductions across multiple cities. A similar pattern is observed for near-surface relative humidity (right panel in Fig. 6), with general reductions in urban areas across most models and cities, particularly during summer; however, the magnitude of these reductions varies substantially between cities and models. Bulk models generally show smaller urban–rural contrasts, and in some cases, especially REMO2020-2-2-iMOVE, CNRM-ALADIN64E1 and RACMO23E, even present positive values, indicating higher relative humidity in urban areas than in their rural surroundings. WRF451Q again shows a more pronounced urban–rural contrast compared with the other bulk models, probably due to the dominant urban fraction treatment.

ROAM-NBS and ICON-CLM-202407-1-1 show nearly identical results for the four variables analyzed, since both share the same atmosphere and land surface model, with the only difference being that ROAM-NBS is coupled to the NEMO ocean model for the North and Baltic Sea (Maurer et al., 2026). However, their smoothed urban fraction values result in only four cities being detected, making it difficult to generalize the results or compare them with those from the other models. CCLM6-0-1-URB and CCLM6-0-1-URB-ESG models also show similar results for the four variables analyzed; however, in this case, the number of cities represented by each model differs, which is associated with their different land-cover representations.

Fig. 7 shows spatial maps of the ensemble mean results for both sub-ensembles and the four analysed variables. Note that these ensemble means might be biased towards the behaviour of particular model families which contribute more members to the ensemble. Still, it provides a summary of model behaviour which can be used to identify spatial patterns. The behaviour of specific model families or ensemble members can then be disentangled from Fig.s 5 and 6. For temperature, the nocturnal (tasmin) UHI exhibits higher values than the diurnal (tasmax) UHI, particularly in summer and in coastal cities, where the proximity of urban areas to the sea compared to surrounding rural areas enhances this contrast. During winter, nocturnal (tasmin) UHI displays a latitudinal gradient, with higher values in southern Europe. During summer, continental cities, particularly those in central Europe, exhibit larger diurnal (tasmax) UHI intensities, suggesting that the UHI intensity may be moderated by the presence of the sea in coastal cities during the day. In contrast, several cities located in arid and semi-arid environments, as well as some Mediterranean cities, experience an urban cool island effect, with negative diurnal (tasmax) UHI intensities during summer. This effect is more pronounced, or in some cases only detected, in the UCM models. In general, the UCM sub-ensemble exhibits higher urban–rural contrasts than the bulk models for both nocturnal and diurnal UHI.

The urban-rural contrasts in near-surface wind speed (sfcWind) are larger during winter and show a clear latitudinal pattern, with higher values in northern European regions. The largest absolute reductions are observed in cities across England and northern Europe, which is the area with stronger wind and wind variability. In some cities, such as Valencia and Antalya, the two sub-ensembles even show opposite signals during winter, highlighting the stronger sensitivity of wind response to the urban scheme. Gothenburg, Helsinki, and Riga exhibit contrasting signals, with higher wind speeds in urban areas.

For near-surface relative humidity (hurs), the UDI is more pronounced during the summer months, again displaying a clear spatial pattern, resembling the temperature pattern with stronger UDI decreases in northern regions with stronger UHI values. Coastal cities experience a less pronounced UDI effect due to sea-breeze circulation, which transports moisture from the sea to the land (Huang and Song, 2023). UCM models simulate larger reductions in urban areas, particularly in winter months. The reductions are more pronounced in central European inland cities located far from the sea. In arid regions of North Africa, the urban–rural contrast signal differs, likely because urban areas located closer to the sea than the surrounding rural areas can experience higher humidity levels.

Finally, Fig. 8 shows the urban–rural contrast classified by season, geographical location (coastal, inland, and mountain), RCM urban approach (UCM or bulk), and IPCC AR6 regions. Apart from the summary boxplots, the urban–rural contrast for each individual city is represented as points, with different colors indicating different RCMs. The RCMs are positioned at separate x-axis locations, enabling visualization of both inter- and intra-model spread within each classification.

Inland cities exhibit the highest diurnal (tasmax) UHI intensities in summer, whereas coastal cities show stronger nocturnal (tasmin) UHI intensities in winter. As already mentioned, this pattern reflects the moderating effect of the sea in urban areas, which are

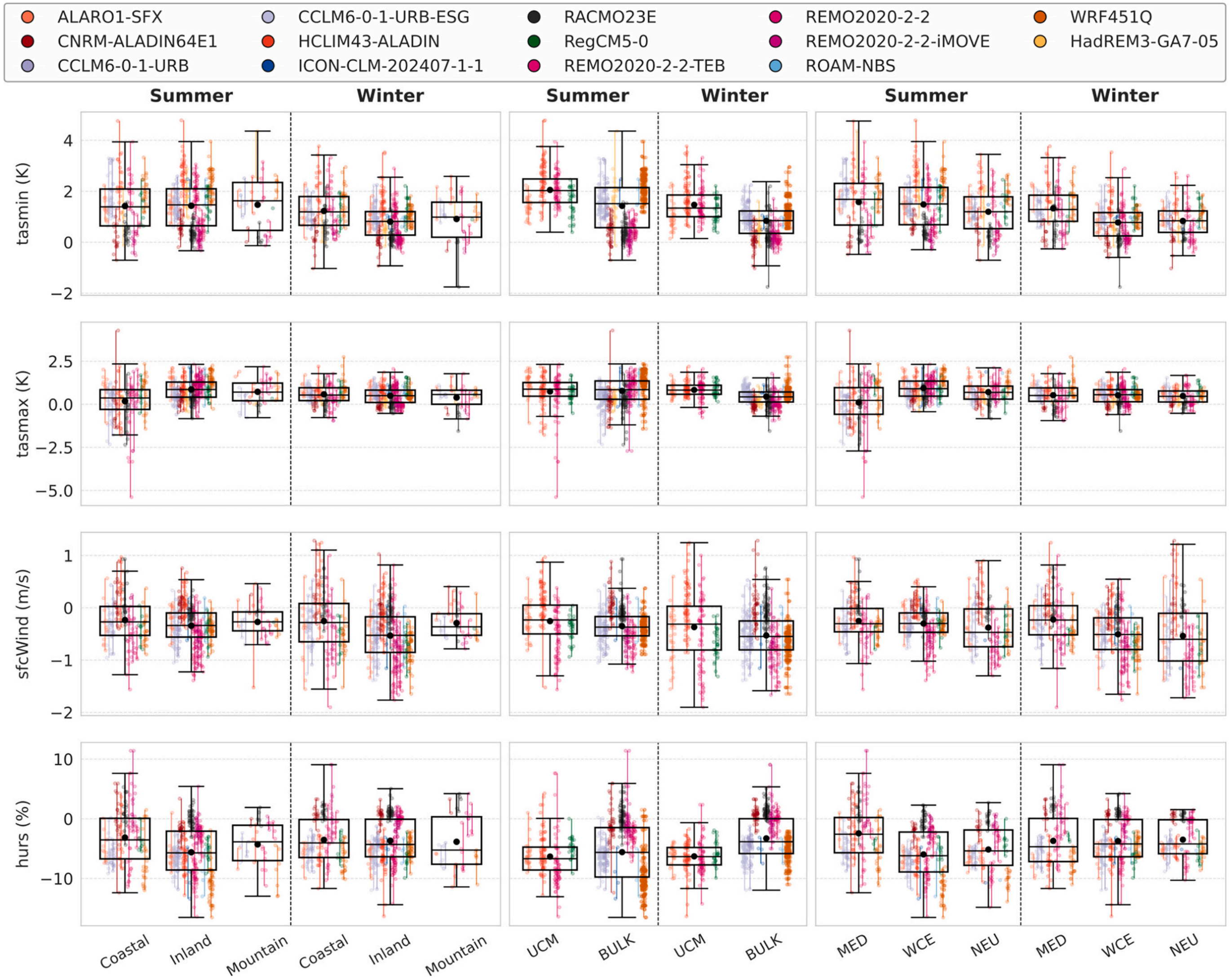

Fig. 8. Urban-rural contrasts for the four variables (rows) for the stations classified following different criteria. From left to right: city classification based on geographical location (coastal, inland, and mountain), RCM classification based on urban scheme (UCM or bulk) and IPCC AR6 regions. Each point corresponds to the urban–rural contrast for each city, with a different color representing each RCM. Each RCM is shown in a different x-axis position. Yerevan and Nizhny Novgorod cities were excluded from the AR6 analysis because they are the only cities classified within the WCA and EUU regions, respectively. Black boxes span the interquartile range (25th to 75th percentiles), with the median indicated as a horizontal line, for all stations and RCMs within each category. Fig.s 10SM–12SM in the Supplementary Material extend this fig. by assigning a numerical identifier to each RCM to identify which model corresponds to each data point.

generally located closer to the coast than their surrounding rural areas, reducing daytime heating and enhancing nocturnal cooling contrasts. Inland cities also exhibit stronger reductions in near-surface wind speed (sfcWind) during winter and in near-surface relative humidity (hurs) during summer compared with coastal cities, likely due to the moderating influence of sea breezes, increased storm activity in winter, and higher moisture availability near the coast.

UCM models tend to simulate higher nocturnal (tasmin) UHI intensities than bulk models in both summer and winter, with the exception of WRF451Q and CCLM6-0-1-URB. The diurnal (tasmax) UHI intensity is similar or more pronounced in bulk models during summer, and, to a lesser extent, more pronounced in UCM models during winter. For near-surface wind speed (sfcWind), reductions in urban areas are more pronounced in bulk approaches in both summer and winter, although the results are less consistent.The UDI effect is stronger in most UCM models in both summer and winter than in bulk models, except for WRF451Q and CCLM6-0-1-URB, which shifts the ensemble mean toward stronger summer signals.

When the results are aggregated by IPCC AR6 regions, some patterns emerge since they are aligned with the latitudinal gradients we showed in previous fig.s. Nocturnal (tasmin) UHI intensity is strongest in the Mediterranean (MED), followed by Western Central Europe (WCE) and Northern Europe (NEU), exhibiting a clear north–south gradient consistent with Fig. 7. Diurnal (tasmax) UHI intensity peaks in the central WCE region, also in agreement with Fig. 7. Reductions in near-surface wind speed (sfcWind) are largest in NEU, followed by WCE and MED, indicating a south–north gradient. For relative humidity (hurs), the largest reductions occur during summer in the WCE and NEU regions and during winter all regions show similar results.

Finally, as already illustrated in Fig.s 5 and 6, we can see that the different RCMs are a major source of uncertainty, leading to differences larger than those among cities with different degrees of continentality or in different latitudes. Although not explicitly factored by RCM, this classification can be seen in the central panels of Fig. 8 (UCM vs bulk), since this representation splits cleanly across RCMs and includes all cities for each of them. We can see how models in the bulk ensemble can have very different behaviour (e.g. WRF451Q and REMO2020-2-2 variants), acting as a major driver of the uncertainty in the results. This result further confirms the need to establish multi-city and multi-model ensembles as a standard practice in urban climate analyses, along with working towards improving the models and reducing uncertainties. For the latter, trustworthy observational databases for urban and surrounding areas are essential.

5. Discussion and conclusion

This paper presents the first coordinated evaluation of urban climate in the new ERA5-driven EURO-CORDEX simulations, part of the CORDEX-CMIP6 downscaling exercise (Fernandez et al., 2026). We build on the work carried out by the FPS URB-RCC for the previous CMIP5-driven generation (Diez-Sierra et al., 2025; Langendijk et al., 2026; Langendijk et al., 2024; Zazulie et al., 2026). This unique multi-model ensemble represents a significant step forward, particularly in terms of the availability and consistency of urban information across participating institutions, by providing urban fraction data for all models, as well as larger presence and advances in urban parameterization schemes. This enables the application of a consistent methodology for delineating urban and rural areas across the entire ensemble and the sampled cities, allowing for a robust and comparable assessment of urban–rural contrasts (Diez-Sierra et al., 2025). Consequently, this ensemble provides, for the first time, a coordinated framework to evaluate urban imprints at the continental scale across the EURO-CORDEX domain (covering Europe and parts of North Africa), including nearly all participating models.

Key advances of this new generation of models include: (1) the explicit representation of urban areas through different urban parameterizations, comprising four RCMs with urban canopy models (UCMs) and ten RCMs with bulk schemes, among which TERRA_URB, an improved bulk scheme, produces results comparable to those of the UCMs; (2) an ensemble of 14 model configurations, providing a more robust estimate of uncertainty; and (3) the inclusion of an RCM with an interactive vegetation scheme (REMO2020-2-2-iMOVE) and its land-use/land-cover change variant (REMO2020-2-2-iMOVE-LUC), which accounts for historical LULC changes and future SSP-consistent projections with evolving urban areas, representing a significant advancement for assessing urban impacts in both historical simulations and future projections.

Despite these advances, several important limitations remain. The grid spacing of the simulations (~12,5 km) is still relatively coarse for resolving the complex spatial structure of urban areas, limiting the representation of intra-urban heterogeneity and local-scale processes. In addition, the ensemble partly relies on outdated land use and land cover datasets (ranging from the early 1990s to around 2015), which may lead to substantial underestimation or misrepresentation of urban extent and impervious surfaces in different periods for different models. The heterogeneity in land-cover datasets used across models, as well as differences in their reference periods, further contributes to inter-model differences in the simulated urban imprint and complicates their evaluation against observations. Consequently, part of the spread in the simulated urban–rural contrasts across the ensemble may arise not only from differences in urban parameterizations but also from inconsistencies in the underlying land-surface characterization. These aspects should therefore be considered when interpreting inter-model differences and assessing the robustness of simulated urban climate signals. Additionally, the differing treatment of anthropogenic heat across the various urban schemes, with some lacking any representation of anthropogenic heat, constitutes another source of uncertainty.

Within this context, the analysis also highlights important differences in the urban parameterizations implemented by individual models and the potential interdependencies between them, which should be taken into account when interpreting the ensemble within a probabilistic framework. For this purpose, two sub-ensembles were defined: a bulk and a UCM sub-ensemble, reflecting their different representations of urban processes. Note, however, that even within these sub-ensembles, each of the members is not completely independent from the rest, and the probabilistic framework (e.g. considering ensemble means) is compromised by the presence of different model variants (Fernandez et al., 2026). The root in the model naming can be a guidance to identify some of these variants, such as those starting with REMO, CCLM or ICON, but others are less obvious (TSMP, GCOAST and ROAM are also variants of CCLM and ICON). In this work, we considered only a few representatives from each model family and we avoided as much as possible cross-model averages, favouring the display of individual model results.

We showed that UCM models tend to simulate larger nocturnal UHI intensities in both summer and winter, with HCLIM43-ALADIN showing the largest contrasts among the models analyzed. These differences are particularly pronounced in winter, where several bulk models that do not account for anthropogenic heat show a reduced diurnal UHI or even negative values. The bulk-based WRF451Q model, which uses a binary urban fraction approach, simulates nocturnal UHI intensities comparable to those produced by UCM models. Similarly, CCLM6-0-1-URB (and its ESG version), using the TERRA_URB bulk scheme, shows results comparable to those of the UCM models. Over the European domain, a latitudinal gradient in nocturnal UHI intensity is detectable, with higher values across the southern regions. For diurnal UHI intensity, both sub-ensembles show broadly similar results during summer, whereas in winter UCM models and only WRF451Q from the bulk models generally simulate higher UHI intensities. Bulk models tend to exhibit stronger seasonality than UCM ones.

During summer, several cities located in arid or semi-arid regions exhibit the urban cool island effect (Bushenkova et al., 2024; Lazzarini et al., 2013; Rasul et al., 2016; Yang et al., 2017), where sparsely vegetated urban surrounding areas become warmer than urban areas during daytime due to strong surface heating, while urban materials and shading may limit daytime temperatures within the city. This effect is more intense and in some cases only detected by the UCM models. Negative diurnal UHI intensities are also observed in several coastal cities with warm summers, which likely arise from the closer proximity of urban areas to the sea compared to surrounding rural areas.

For near-surface wind speed, both sub-ensembles generally simulate reductions in urban areas relative to rural surroundings, reflecting the increased surface roughness associated with urban structures or specific parameter settings for the urban fraction, with bulk models generally simulating stronger reductions. WRF451Q from the bulk sub-ensemble and REMO2020-2-2-TEB from the UCM sub-ensemble show the largest reductions in near-surface wind speed across multiple cities. The magnitude of wind speed reduction is typically larger during winter and shows a latitudinal gradient, with stronger effects in the windier northern Europe. In some cities, and particularly for models such as HCLIM43-ALADIN, CNRM-ALADIN64E1, and RACMO23E, the two sub-ensembles even produce opposite signals (increased wind speed in urban areas), highlighting the strong sensitivity of wind responses to the representation of urban processes.

For near-surface relative humidity, UCM models generally simulate larger reductions in urban areas during both summer and winter. However, in summer the relatively strong reductions simulated by WRF451Q shift the bulk sub-ensemble towards the values simulated by UCM models. Again CCLM6-0-1-URB (and the ESG version) show results comparable to those of UCM models. The reduction in relative humidity in urban areas is typically stronger during summer in bulk models and exhibits a pronounced north–south gradient, with larger decreases in northern regions. The strongest reductions are found in central European inland cities located far from the sea. In contrast, in arid and semi-arid regions of North Africa the signal differs: urban areas that are located closer to the sea than their surrounding rural areas may experience higher humidity levels.

The two versions of REMO2020-2-2 (with and without TEB) enable a direct and consistent comparison between the bulk and UCM urban approaches using the same model setup. For nocturnal UHI, the UCM version shows higher urban–rural contrasts across all cities. In contrast, for diurnal UHI, the bulk version produces negligible or negative UHI intensities during winter and exhibits a more pronounced seasonal cycle with higher values in summer, whereas the UCM version maintains substantial UHI intensities throughout the year. Near-surface wind speed shows urban reductions in most cities, with greater variability across cities in the UCM version. Reductions in relative humidity are significantly larger in the UCM version for both summer and winter.

It is important to note that the differences in urban–rural contrasts between the two sub-ensembles are of comparable magnitude, and in some cases even larger, particularly for temperature and relative humidity, than those associated with their geographical location or IPCC AR6 region. Moreover, the RCM configuration alone is among the major sources of uncertainty. This underscores that the choice of urban parameterization is a key factor influencing the results and that the use of multi-model ensembles is key to address the urban-rural contrast uncertainties.

The evaluation against observations from fourteen cities does not reveal a clear added value of UCMs relative to bulk schemes. The current approach for automatically selecting urban and rural observations based on administrative city boundaries has notable limitations, even though we have used some of the highest-density observational datasets available in Europe. Point observations cannot be directly compared with model grid-cell averages due to their different spatial representativeness, and, more importantly, stations may not exhibit the characteristics of their location in the model. For instance, many urban stations are actually located in parks, airports, or other low-density suburban environments that may not be representative of dense urban conditions (Peterson, 2003), while many rural stations represent mixed rural and urban influences (e.g. villages). Therefore, the conclusions drawn from the observational evaluation should be regarded as qualitative rather than quantitative, as the limited representativeness of the available urban and rural stations prevents a robust assessment of the relative performance of the RCMs.

These findings highlight the urgent need for alternative methodologies to evaluate urban climate simulations against observations, enabling more robust assessments of model skill in representing urban processes rather than merely inter-model comparisons. For example, evaluating the urban representation in RCMs over Europe would greatly benefit from the availability of long-term, high-quality observational datasets for European cities. This is, of course, a general problem (Langendijk et al., 2026) that should be tackled at global scale. Alternatively, such evaluations could consider the explicit land use/land cover (LULC) at the location of the stations rather than directly comparing urban and rural stations (Luo and Lau, 2019), or leverage other reference sources, such as remote sensing–based datasets (Bechtel et al., 2017; Venter et al., 2020; Zhao et al., 2014).

Future studies should further explore the potential of satellite observations for the evaluation of urban climate simulations, despite their limitations, including the measurement of land surface rather than near-surface air temperature and discontinuous spatio-temporal coverage due to satellite overpass frequency and cloud contamination (Chakraborty et al., 2024; Voogt and Oke, 2003). In addition, the increasing availability of citizen weather observations worldwide offers considerable potential to complement conventional monitoring networks through data fusion approaches, thereby improving the spatial coverage and representativeness of urban observations (Marquès and Messier, 2025). Integrating satellite products, citizen weather observations, and conventional station networks could therefore contribute to the development of more comprehensive observational datasets for the evaluation and validation of urban climate models.

In Paris, where the density and distribution of observational stations adequately capture the urban–rural contrast, several bulk models, including CNRM-ALADIN64E1, RACMO23E, and REMO2020-2-2, substantially underestimate the nocturnal UHI. For the diurnal UHI, bulk models exhibit a more pronounced seasonal cycle than observed, whereas UCM models better reproduce the observed cycle, showing higher UHI values in winter and moderated values in summer, highlighting their improved performance. Literature reviews for several of the 14 cities further indicate that UCM models generally provide a more accurate representation of both UHI and urban dry island effects, while also emphasizing that the urban–rural contrast is often poorly captured by existing observational networks in many cities.

Overall, for urban climate analyses we recommend relying on the UCM models or enhanced bulk models, such as the CCLM6-0-1-URB variants using TERRA_URB, which have explicit representations of key urban processes. Bulk models, and especially those representing dominant land use and urban categories (WRF451Q), may have a strong sensitivity to the presence of urban areas, and show clear urban climate islands, but miss key processes governing them and may respond to climate changes quite differently than more detailed UCMs.

Despite the limitations of the RCMs and observational data sets, this work provides a unique contribution by establishing a framework to evaluate urban imprints using RCMs and by offering a reference baseline for investigating cities under climate change using EURO-CORDEX CMIP6 downscaled projections, as well as for future high-resolution studies, such as the Flagship Pilot Studies (FPS) using convection-permitting regional climate models (CPRCMs) or next-generation modelling frameworks. In particular, forthcoming CORDEX-CORE (Coppola et al., 2021; Giorgi et al., 2022) simulations within CORDEX-CMIP6 will enable extending this analysis to other regions worldwide.

CRediT authorship contribution statement

Javier Diez-Sierra: Writing – original draft, Visualization, Validation, Supervision, Methodology, Investigation, Formal analysis, Data curation, Conceptualization. **Natalia Zazulie:** Writing – original draft, Validation, Supervision, Methodology, Investigation, Conceptualization. **Gaby S. Langendijk:** Writing – review & editing, Validation, Supervision, Methodology. **Yaiza Quintana:** Writing – review & editing, Visualization, Validation, Formal analysis, Data curation. **Marianna Adinolfi:** Writing – review & editing, Validation. **May Bohmann:** Writing – review & editing, Validation. **Lars Buntemeyer:** Writing – review & editing, Validation. **Erasmo Buonomo:** Writing – review & editing, Validation. **Steven Caluwaerts:** Writing – review & editing, Validation, Supervision. **Angelo Campanale:** Writing – review & editing, Validation. **Rita M. Cardoso:** Writing – review & editing, Validation. **David Carvalho:** Writing – review & editing, Validation. **Ana Casanueva:** Writing – review & editing, Validation. **Matthias Demuzere:** Writing – review & editing, Validation, Methodology. **Theodore Endreny:** Writing – review & editing, Validation, Supervision. **Jesús Fernández:** Writing – review & editing, Validation, Supervision, Methodology. **Nicolas Ghilain:** Writing – review & editing, Validation. **Klaus Goergen:** Writing – review & editing, Validation. **Tomas Halenka:** Writing – review & editing, Validation, Supervision. **Peter Hoffmann:** Writing – review & editing, Validation, Supervision. **Eleni Katragkou:** Writing – review & editing, Validation, Supervision. **Sven Kotlarski:** Writing – review & editing, Validation, Supervision. **Patrick Ludwig:** Writing – review & editing, Validation. **Vera Maurer:** Writing – review & editing, Validation. **Josipa Milovac:** Writing – review & editing, Validation, Supervision. **Rita Nogherotto:** Writing – review & editing, Validation, Methodology. **Vasileios Pavlidis:** Writing – review & editing, Validation. **Joni-Pekka Pietikäinen:** Writing – review & editing, Validation, Supervision. **Mario Raffa:** Writing – review & editing, Validation. **Diana Rechid:** Writing – review & editing, Validation, Supervision. **Jan-Peter Schulz:** Writing – review & editing, Validation. **Fien Serras:** Writing – review & editing, Validation. **Andres Simon-Moral:** Writing – review & editing, Validation. **Pedro M.M. Soares:** Writing – review & editing, Validation. **Stefan Sobolowski:** Writing – review & editing, Validation, Supervision. **Claas Teichmann:** Writing – review & editing, Validation. **Kobe Vandelanotte:** Writing – review & editing, Validation. **Inne Vanderkelen:** Writing – review & editing, Validation. **Fuxing Wang:** Writing – review & editing, Validation.

Declaration of competing interest

All authors declare that they have no known financial or personal relationships with other people or organizations that could inappropriately influence or bias the work reported in this paper.

The authors confirm that they have no competing interests to declare.

Acknowledgments

The authors gratefully acknowledge the research data exchange infrastructure and services provided by the Jülich Supercomputing Centre, Germany, as part of the JSC Cloud. We acknowledge all participating institutions for their voluntary effort and contribution to EURO-CORDEX. N.Z., S.S., T.H. and J.F. acknowledge support from Horizon Europe project Impetus4Change (I4C, grant id. 101081555). N.Z. acknowledges funding from Ministero dell'Università e della Ricerca under the call Fondo Italiano per la Scienza 2022-2023 (FIS-2) for the project "Mediterranean Extreme Events and Tipping elements in a changing climate on multiple spatiotemporal scales", grant number FIS-2023-00159, CUP: D53C24005450001. M.D., A.C, M.R. and M.A. acknowledge support from the European Union's HORIZON Research and Innovation Actions under grant agreement No 101137851, project CARMINE (Climate-Resilient Development Pathways in Metropolitan Regions of Europe, https://carmine-project.eu). A.C., G.S.L. and J.F. acknowledge support from Grant PID2023-149997OA-I00 (PROTECT) funded by MICIU/AEI/10.13039/501100011033 and by ERDF/EU. E.K. and V.P. acknowledge support from H.F.R.I "Basic research Financing (Horizontal support of all Sciences)" under the National Recovery and Resilience Plan "Greece 2.0" funded by the European Union—NextGenerationEU (H.F.R.I. Project Number:14696). Their work was supported by computational time granted from the National Infrastructures for Research and Technology S.A. (GRNET S.A.) in the National HPC facility - ARIS - under project ID pr017036_thin. T.H. acknowledges support partly by the Project OP JAK "Natural and anthropogenic georisks" No.CZ.02.01.014/0022_008/0004605. We are grateful to Christina Pop, who performed the REMO-iMOVE simulations, supported by the project OptFor-EU within the Horizon Europe research and innovation programme under grant agreement no. 101060554. For the REMO-iMOVE simulations we used resources of the Deutsches Klimarechenzentrum (DKRZ) granted by its Scientific Steering Committee (WLA) under project ID bg1370. J.M. acknowledges funding by the Ministry for the Ecological Transition and the Demographic Challenge (MITECO) and the European Commission NextGeneration EU (Regulation EU 2020/2094), through CSIC's Interdisciplinary Thematic Platform Clima (PTI-Clima).

Appendix A. Supplementary data

Supplementary data to this article can be found online at https://doi.org/10.1016/j.uclim.2026.103103.

Data availability

EURO-CORDEX data will be publicly available through the Earth System Grid Federation. The code for reproducing the results is available on GitHub at https://github.com/euro-cordex/urban-evaluation.

References

Adinolfi, M., Raffa, M., Reder, A., Mercogliano, P., 2023. Investigation on potential and limitations of ERA5 Reanalysis downscaled on Italy by a convection-permitting model. Clim. Dyn. 61, 4319–4342. https://doi.org/10.1007/s00382-023-06803-w.

Argüeso, D., Di Luca, A., Evans, J.P., 2016. Precipitation over urban areas in the western Maritime Continent using a convection-permitting model. Clim. Dyn. 47, 1143–1159. https://doi.org/10.1007/s00382-015-2893-6.

Arnds, D., Böhner, J., Bechtel, B., 2017. Spatio-temporal variance and meteorological drivers of the urban heat island in a European city. Theor. Appl. Climatol. 128, 43–61. https://doi.org/10.1007/s00704-015-1687-4.

Baidar, S., Bonin, T., Choukulkar, A., Brewer, A., Hardesty, M., 2020. Observation of the Urban Wind Island Effect. EPJ Web Conf. 237, 06009. https://doi.org/10.1051/epjconf/202023706009.

Bechtel, B., Zakšek, K., Oßenbrügge, J., Kaveckis, G., Böhner, J., 2017. Towards a satellite based monitoring of urban air temperatures. Sustain. Cities Soc. 34, 22–31. https://doi.org/10.1016/j.scs.2017.05.018.

Best, M.J., 2005. Representing urban areas within operational numerical weather prediction models. Bound.-Layer Meteorol. 114, 91–109. https://doi.org/10.1007/s10546-004-4834-5.

Best, M.J., Pryor, M., Clark, D.B., Rooney, G.G., Essery, R.L.H., Ménard, C.B., Edwards, J.M., Hendry, M.A., Porson, A., Gedney, N., Mercado, L.M., Sitch, S., Blyth, E., Boucher, O., Cox, P.M., Grimmond, C.S.B., Harding, R.J., 2011. The Joint UK Land Environment Simulator (JULES), model description – Part 1: Energy and water fluxes. Geosci. Model Dev. 4, 677–699. https://doi.org/10.5194/gmd-4-677-2011.

Bueno, B., Pigeon, G., Norford, L.K., Zibouche, K., Marchadier, C., 2012. Development and evaluation of a building energy model integrated in the TEB scheme. Geosci. Model Dev. 5, 433–448. https://doi.org/10.5194/gmd-5-433-2012.

Burian, S.J., Shepherd, J.M., 2005. Effect of urbanization on the diurnal rainfall pattern in Houston. Hydrol. Process. 19, 1089–1103. https://doi.org/10.1002/hyp.5647.

Bushenkova, A., Soares, P.M.M., Johannsen, F., Lima, D.C.A., 2024. Towards an improved representation of the urban heat island effect : A multi-scale application of XGBoost for madrid. Urban Clim. 55, 101982. https://doi.org/10.1016/j.uclim.2024.101982.

Campanale, A., Adinolfi, M., Raffa, M., Schulz, J.-P., Mercogliano, P., 2025. Investigating urban heat islands over Rome and Milan during a summer period through the TERRA_URB parameterization in the ICON model. Urban Clim. 60, 102335. https://doi.org/10.1016/j.uclim.2025.102335.

Chakraborty, T., Venter, Z.S., Demuzere, M., Zhan, W., Gao, J., Zhao, L., Qian, Y., 2024. Large disagreements in estimates of urban land across scales and their implications. Nat Commun 15, 9165. https://doi.org/10.1038/s41467-024-52241-5.

Chen, B., Wang, W., Dai, W., Chang, M., Wang, X., You, Y., Zhu, W., Liao, C., 2021. Refined urban canopy parameters and their impacts on simulation of urbanization-induced climate change. Urban Clim. 37, 100847. https://doi.org/10.1016/j.uclim.2021.100847.

Childs, P.P., Raman, S., 2005. Observations and Numerical Simulations of Urban Heat Island and Sea Breeze Circulations over New York City. Pure Appl. Geophys. 162, 1955–1980. https://doi.org/10.1007/s00024-005-2700-0.

Coppola, E., Sobolowski, S., Pichelli, E., Raffaele, F., Ahrens, B., Anders, I., Ban, N., Bastin, S., Belda, M., Belusic, D., Caldas-Alvarez, A., Cardoso, R.M., Davolio, S., Dobler, A., Fernandez, J., Fita, L., Fumiere, Q., Giorgi, F., Goergen, K., Güttler, I., Halenka, T., Heinzeller, D., Hodnebrog, Ø., Jacob, D., Kartsios, S., Katragkou, E., Kendon, E., Khodayar, S., Kunstmann, H., Knist, S., Lavín-Gullón, A., Lind, P., Lorenz, T., Maraun, D., Marelle, L., van Meijgaard, E., Milovac, J., Myhre, G., Panitz, H.-J., Piazza, M., Raffa, M., Raub, T., Rockel, B., Schär, C., Sieck, K., Soares, P.M.M., Somot, S., Srnec, L., Stocchi, P., Tölle, M.H., Truhetz, H., Vautard, R., de Vries, H., Warrach-Sagi, K., 2020. A first-of-its-kind multi-model convection permitting ensemble for investigating convective phenomena over Europe and the Mediterranean. Clim. Dyn. 55, 3–34. https://doi.org/10.1007/s00382-018-4521-8.

Coppola, E., Raffaele, F., Giorgi, F., Giuliani, G., Xuejie, G., Ciarlo, J.M., Sines, T.R., Torres-Alavez, J.A., Das, S., di Sante, F., Pichelli, E., Glazer, R., Müller, S.K., Abba Omar, S., Ashfaq, M., Bukovsky, M., Im, E.-S., Jacob, D., Teichmann, C., Remedio, A., Remke, T., Kriegsmann, A., Bülow, K., Weber, T., Buntemeyer, L., Sieck, K., Rechid, D., 2021. Climate hazard indices projections based on CORDEX-CORE, CMIP5 and CMIP6 ensemble. Clim. Dyn. 57, 1293–1383. https://doi.org/10.1007/s00382-021-05640-z.

Diez-Sierra, J., Iturbide, M., Gutiérrez, J.M., Fernández, J., Milovac, J., Cofiño, A.S., Cimadevilla, E., Nikulin, G., Levavasseur, G., Kjellström, E., Bülow, K., Horányi, A., Brookshaw, A., García-Díez, M., Pérez, A., Baño-Medina, J., Ahrens, B., Alias, A., Ashfaq, M., Bukovsky, M., Buonomo, E., Caluwaerts, S., Chou, S.C., Christensen, O.B., Ciarlò, J.M., Coppola, E., Corre, L., Demory, M.-E., Djurdjevic, V., Evans, J.P., Fealy, R., Feldmann, H., Jacob, D., Jayanarayanan, S., Katzfey, J., Keuler, K., Kittel, C., Kurnaz, M.L., Laprise, R., Lionello, P., McGinnis, S., Mercogliano, P., Nabat, P., Önol, B., Ozturk, T., Panitz, H.-J., Paquin, D., Pieczka, I., Raffaele, F., Remedio, A.R., Scinocca, J., Sevault, F., Somot, S., Steger, C., Tangang, F., Teichmann, C., Termonia, P., Thatcher, M., Torma, C., Meijgaard, E., Vautard, R., Warrach-Sagi, K., Winger, K., Zittis, G., 2022. The Worldwide C3S CORDEX Grand Ensemble: A Major Contribution to Assess Regional Climate Change in the IPCC AR6 Atlas. Bull. Am. Meteorol. Soc. 103, E2804–E2826. https://doi.org/10.1175/BAMS-D-22-0111.1.

Diez-Sierra, J., Quintana, Y., Langendijk, G.S., Milovac, J., Demuzere, M., Nogherotto, R., Pietikäinen, J.-P., Rechid, D., Zazulie, N., Solman, S.A., Fernández, J., 2025. A global CORDEX-based dataset delineating urban areas and their surroundings to assess climate change in megacities. Sci. Data 12, 1961. https://doi.org/10.1038/s41597-025-06257-1.

Doan, Q.-V., Chen, F., Kusaka, H., Dipankar, A., Khan, A., Hamdi, R., Roth, M., Niyogi, D., 2022. Increased Risk of Extreme Precipitation Over an Urban Agglomeration With Future Global Warming. Earths. Future 10. https://doi.org/10.1029/2021EF002563 e2021EF002563.

Dong, Y., Varquez, A.C.G., Kanda, M., 2017. Global anthropogenic heat flux database with high spatial resolution. Atmos. Environ. 150, 276–294. https://doi.org/10.1016/j.atmosenv.2016.11.040.

Droste, A.M., Steeneveld, G.J., Holtslag, A.A.M., 2018. Introducing the urban wind island effect. Environ. Res. Lett. 13, 094007. https://doi.org/10.1088/1748-9326/aad8ef.

EURO-CORDEX, 2023. EURO-CORDEX-CMIP6 RCM component description. Zenodo. https://doi.org/10.5281/ZENODO.8388778.

Global Human Settlement - Urban Centre database R2024A European Commission, n.d. URL https://human-settlement.emergency.copernicus.eu/ghs_ucdb_2024.php (accessed 2.3.26).

Fenner, D., Meier, F., Scherer, D., Polze, A., 2014. Spatial and temporal air temperature variability in Berlin, Germany, during the years 2001–2010. In: Urban Clim., ICUC8: The 8th International Conference on Urban Climate and the 10th Symposium on the Urban Environment 10, pp. 308–331. https://doi.org/10.1016/j.uclim.2014.02.004.

Fernandez, J., Diez-Sierra, J., Buntemeyer, L., Goergen, K., Nikulin, G., Kotlarski, S., Teichmann, C., et al., 2026. Advancing regional climate modelling in Europe: evaluation of the new ERA5-driven EURO-CORDEX-CMIP6 ensemble. Geosci, Model Dev in prep.

Founda, D., Santamouris, M., 2017. Synergies between Urban Heat Island and Heat Waves in Athens (Greece), during an extremely hot summer (2012). Sci. Rep. 7, 10973. https://doi.org/10.1038/s41598-017-11407-6.

Founda, D., Pierros, F., Petrakis, M., Zerefos, C., 2015. Interdecadal variations and trends of the Urban Heat Island in Athens (Greece) and its response to heat waves. Atmospheric Res. 161–162, 1–13. https://doi.org/10.1016/j.atmosres.2015.03.016.

Garbero, V., Milelli, M., Bucchignani, E., Mercogliano, P., Varentsov, M., Rozinkina, I., Rivin, G., Blinov, D., Wouters, H., Schulz, J.-P., Schättler, U., Bassani, F., Demuzere, M., Repola, F., 2021. Evaluating the Urban Canopy Scheme TERRA_URB in the COSMO Model for Selected European Cities. Atmosphere 12. https://doi.org/10.3390/atmos12020237.

Geyer, Beate, Campanale, Angelo, Churiulin, Evgenii, Feldmann, Hendrik, Goergen, Klaus, Hagemann, Stefan, Ho-Hagemann, Ha Thi Minh, Karadan Muhammed, Muhshif, Keuler, Klaus, Pavel, Khain, Lawand, Divyaja, Maurer, Vera, Petrov, Sergei, Poll, Stefan, Purr, Christopher, Russo, Emmanuele, Schubert-Frisius, Martina, Schulz, Jan-Peter, Singh, Shweta, Steger, Christian, Truhetz, Heimo, 2026. Optimisation of ICON-CLM for the EURO-CORDEX domain: developments, sensitivities, tuning. Geosci. Model Dev. 19 (12), 5439–5490.

Giorgi Jr., F., 2015. Regional Dynamical Downscaling and the CORDEX Initiative. Annu. Rev. Environ. Resour. 40, 467–490. https://doi.org/10.1146/annurev-environ-102014-021217.

Giorgi, F., Coppola, E., Jacob, D., Teichmann, C., Omar, S.A., Ashfaq, M., Ban, N., Bülow, K., Bukovsky, M., Buntemeyer, L., Cavazos, T., Ciarlo, J., Rocha, R.P., Das, S., Sante, F., Evans, J.P., Gao, X., Giuliani, G., Glazer, R.H., Hoffmann, P., Im, E.-S., Langendijk, G., Lierhammer, L., Llopart, M., Mueller, S., Luna-Nino, R., Nogherotto, R., Pichelli, E., Raffaele, F., Reboita, M., Rechid, D., Remedio, A., Remke, T., Sawadogo, W., Sieck, K., Torres-Alavez, J.A., Weber, T., 2022. The CORDEX-CORE EXP-I Initiative: Description and Highlight Results from the Initial Analysis. Bull. Am. Meteorol. Soc. 103, E293–E310. https://doi.org/10.1175/BAMS-D-21-0119.1.

Guerreiro, S.B., Dawson, R.J., Kilsby, C., Lewis, E., Ford, A., 2018. Future heat-waves, droughts and floods in 571 European cities. Environ. Res. Lett. 13, 034009.

Gutiérrez, J.M., Jones, R.G., Narisma, G.T., Alves, L.M., Amjad, M., Gorodetskaya, I.V., Grose, M., Klutse, N.A.B., Krakovska, S., Li, J., Martínez-Castro, D., Mearns, L. O., Mernild, S.H., Ngo-Duc, T., van den Hurk, B., Yoon, J.-H., 2021. Atlas. Clim. Change 2021 Phys. Sci. Basis Contrib. Work. Group Sixth Assess. In: Rep. Intergov. Panel Clim. Change.

Gutowski Jr., W.J., Giorgi, F., Timbal, B., Frigon, A., Jacob, D., Kang, H.-S., Raghavan, K., Lee, B., Lennard, C., Nikulin, G., O'Rourke, E., Rixen, M., Solman, S., Stephenson, T., Tangang, F., 2016. WCRP COordinated Regional Downscaling EXperiment (CORDEX): a diagnostic MIP for CMIP6. Geosci. Model Dev. 9, 4087–4095. https://doi.org/10.5194/gmd-9-4087-2016.

Hamdi, R., Kusaka, H., Doan, Q.-V., Cai, P., He, H., Luo, G., Kuang, W., Caluwaerts, S., Duchêne, F., Van Schaeybroek, B., Termonia, P., 2020. The State-of-the-Art of Urban Climate Change Modeling and Observations. Earth Syst. Environ. 4, 631–646. https://doi.org/10.1007/s41748-020-00193-3.

Han, J.-Y., Baik, J.-J., Lee, H., 2014. Urban impacts on precipitation. Asia-Pac. J. Atmospheric Sci. 50, 17–30. https://doi.org/10.1007/s13143-014-0016-7.

Hoffmann, P., Reinhart, V., Rechid, D., de Noblet-Ducoudré, N., Davin, E.L., Asmus, C., Bechtel, B., Böhner, J., Katragkou, E., Luyssaert, S., 2023. High-resolution land use and land cover dataset for regional climate modelling: historical and future changes in Europe. Earth Syst. Sci. Data 15, 3819–3852. https://doi.org/10.5194/essd-15-3819-2023.

Hofstra, N., Haylock, M., New, M., Jones, P.D., 2009. Testing E-OBS European high-resolution gridded data set of daily precipitation and surface temperature. J. Geophys. Res. Atmospheres 114. https://doi.org/10.1029/2009JD011799.

Holmer, B., Eliasson, I., 1999. Urban–rural vapour pressure differences and their role in the development of urban heat islands. Int. J. Climatol. 19, 989–1009. https://doi.org/10.1002/(SICI)1097-0088(199907)19:9%3C989::AID-JOC410%3E3.0.CO;2-1.

Huang, X., Song, J., 2023. Urban moisture and dry islands: spatiotemporal variation patterns and mechanisms of urban air humidity changes across the globe. Environ. Res. Lett. 18, 103003. https://doi.org/10.1088/1748-9326/acf7d7.

Huang, L., Dong, Q., Song, Y., Tao, Y., Shi, L., Zhao, X., Qi, J., Song, Z., Zheng, Z., Zhang, G., Chew, M.Y.L., Setunge, S., Tu, J., Długogórski, B.Z., 2026. Joint effects of urban heat island and global warming on heatwave risk. Sustain. Cities Soc. 141, 107270. https://doi.org/10.1016/j.scs.2026.107270.

Hundhausen, M., Feldmann, H., Laube, N., Pinto, J.G., 2023. Future heat extremes and impacts in a convection-permitting climate ensemble over Germany. Nat. Hazards Earth Syst. Sci. 23, 2873–2893. https://doi.org/10.5194/nhess-23-2873-2023.

IPCC, 2023. Climate Change 2022 – Impacts, Adaptation and Vulnerability: Working Group II Contribution to the Sixth Assessment Report of the Intergovernmental Panel on Climate Change. Cambridge University Press, Cambridge. https://doi.org/10.1017/9781009325844.

Iturbide, M., Gutiérrez, J.M., Alves, L.M., Bedia, J., Cerezo-Mota, R., Cimadevilla, E., Cofiño, A.S., Di Luca, A., Faria, S.H., Gorodetskaya, I.V., Hauser, M., Herrera, S., Hennessy, K., Hewitt, H.T., Jones, R.G., Krakovska, S., Manzanas, R., Martínez-Castro, D., Narisma, G.T., Nurhati, I.S., Pinto, I., Seneviratne, S.I., van den Hurk, B., Vera, C.S., 2020. An update of IPCC climate reference regions for subcontinental analysis of climate model data: definition and aggregated datasets. Earth Syst. Sci. Data 12, 2959–2970. https://doi.org/10.5194/essd-12-2959-2020.

Iturbide, M., Fernández, J., Gutiérrez, J.M., Pirani, A., Huard, D., Al Khourdajie, A., Baño-Medina, J., Bedia, J., Casanueva, A., Cimadevilla, E., Cofiño, A.S., De Felice, M., Diez-Sierra, J., García-Díez, M., Goldie, J., Herrera, D.A., Herrera, S., Manzanas, R., Milovac, J., Radhakrishnan, A., San-Martín, D., Spinuso, A., Thyng, K.M., Trenham, C., Yelekçi, Ö., 2022. Implementation of FAIR principles in the IPCC: the WGI AR6 Atlas repository. Sci. Data 9, 629. https://doi.org/10.1038/s41597-022-01739-y.

Karlický, J., Huszár, P., Halenka, T., Belda, M., Žák, M., Pišoft, P., Mikšovský, J., 2018. Multi-model comparison of urban heat island modelling approaches. Atmospheric Chem. Phys. 18, 10655–10674. https://doi.org/10.5194/acp-18-10655-2018.

Katragkou, E., Sobolowski, S.P., Teichmann, C., Solmon, F., Pavlidis, V., Rechid, D., Hoffmann, P., Fernandez, J., Nikulin, G., Jacob, D., 2024. Delivering an Improved Framework for the New Generation of CMIP6-Driven EURO-CORDEX Regional Climate Simulations. Bull. Am. Meteorol. Soc. 105, E962–E974. https://doi.org/10.1175/BAMS-D-23-0131.1.

Klein Tank, A.M.G., Wijngaard, J.B., Können, G.P., Böhm, R., Demarée, G., Gocheva, A., Mileta, M., Pashiardis, S., Hejkrlik, L., Kern-Hansen, C., Heino, R., Bessemoulin, P., Müller-Westermeier, G., Tzanakou, M., Szalai, S., Pálsdóttir, T., Fitzgerald, D., Rubin, S., Capaldo, M., Maugeri, M., Leitass, A., Bukantis, A., Aberfeld, R., van Engelen, A.F.V., Forland, E., Mietus, M., Coelho, F., Mares, C., Razuvaev, V., Nieplova, E., Cegnar, T., Antonio López, J., Dahlström, B., Moberg, A., Kirchhofer, W., Ceylan, A., Pachaliuk, O., Alexander, L.V., Petrovic, P., 2002. Daily dataset of 20th-century surface air temperature and precipitation series for the European Climate Assessment. Int. J. Climatol. 22, 1441–1453. https://doi.org/10.1002/joc.773.

Klimiuk, T., Ludwig, P., Sanchez-Benitez, A., Goessling, H.F., Braesicke, P., Pinto, J.G., 2025. The European summer heatwave of 2019 – a regional storyline perspective. Earth Syst. Dyn. 16, 239–255. https://doi.org/10.5194/esd-16-239-2025.

Krayenhoff, E.S., Moustaoui, M., Broadbent, A.M., Gupta, V., Georgescu, M., 2018. Diurnal interaction between urban expansion, climate change and adaptation in US cities. Nat. Clim. Change 8, 1097–1103. https://doi.org/10.1038/s41558-018-0320-9.

Kuchcik, M., Czarnecka, K., Błażejczyk, K., 2024. Urban heat island in Warsaw (Poland): Current development and projections for 2050. Urban Clim. 55, 101901. https://doi.org/10.1016/j.uclim.2024.101901.

Kusaka, H., Hara, M., Takane, Y., 2012. Urban Climate Projection by the WRF Model at 3-km Horizontal Grid Increment: Dynamical Downscaling and Predicting Heat Stress in the 2070's August for Tokyo, Osaka, and Nagoya Metropolises. J. Meteorol. Soc. Jpn. Ser II 90B, 47–63. https://doi.org/10.2151/jmsj.2012-B04.

Kuttler, W., Weber, S., Schonnefeld, J., Hesselschwerdt, A., 2007. Urban/rural atmospheric water vapour pressure differences and urban moisture excess in Krefeld. Germany. Int. J. Climatol. 27, 2005–2015. https://doi.org/10.1002/joc.1558.

Langendijk, G.S., Rechid, D., Jacob, D., 2019. Urban areas and urban–rural contrasts under climate change: what does the EURO-CORDEX ensemble tell us?—investigating near surface humidity in berlin and its surroundings. Atmosphere 10, 730. https://doi.org/10.3390/atmos10120730.

Langendijk, G.S., Rechid, D., Sieck, K., Jacob, D., 2021. Added value of convection-permitting simulations for understanding future urban humidity extremes: case studies for Berlin and its surroundings. Weather Clim. Extrem. 33, 100367. https://doi.org/10.1016/j.wace.2021.100367.

Langendijk, G.S., Rechid, D., Jacob, D., 2022. Improved models, improved information? Exploring how climate change impacts pollen, influenza, and mold in Berlin and its surroundings. Urban Clim. 43, 101159. https://doi.org/10.1016/j.uclim.2022.101159.

Langendijk, G.S., Halenka, T., Hoffmann, P., Adinolfi, M., Aldama Campino, A., Asselin, O., Bastin, S., Bechtel, B., Belda, M., Bushenkova, A., Campanale, A., Chun, K. P., Constantinidou, K., Coppola, E., Demuzere, M., Doan, Q.-V., Evans, J., Feldmann, H., Fernandez, J., Fita, L., Hadjinicolaou, P., Hamdi, R., Hundhausen, M., Grawe, D., Johannsen, F., Milovac, J., Katragkou, E., Kerroumi, N.E.I., Kotlarski, S., Le Roy, B., Lemonsu, A., Lennard, C., Lipson, M., Mandal, S., Muñoz Pabón, L. E., Pavlidis, V., Pietikäinen, J.-P., Raffa, M., Raluy-López, E., Rechid, D., Ito, R., Schulz, J.-P., Soares, P.M.M., Takane, Y., Teichmann, C., Thatcher, M., Top, S., Van Schaeybroeck, B., Wang, F., Yuan, J., 2024. Towards better understanding the urban environment and its interactions with regional climate change - The WCRP CORDEX Flagship Pilot Study URB-RCC. Urban Clim. 58, 102165. https://doi.org/10.1016/j.uclim.2024.102165.

Langendijk, G.S., Fernandez, J., Demuzere, M., Diez-Sierra, J., Quintana, Y., Fita, L., Zazulie, N., Nogherotto, R., Carril, A.F., Chun, K.P., Giuliani, G., Halenka, T., Hoffmann, P., Muñoz, L.E., Pietikäinen, J.-P., Rechid, D., Yuan, J., 2026. Representation of global mega-cities and their urban heat island in CORDEX-CORE regional climate model simulations. Npj Urban Sustain. 6. https://doi.org/10.1038/s42949-025-00325-6.

Lazzarini, M., Marpu, P.R., Ghedira, H., 2013. Temperature-land cover interactions: The inversion of urban heat island phenomenon in desert city areas. Remote Sens. Environ. 130, 136–152. https://doi.org/10.1016/j.rse.2012.11.007.

Le Roy, B., Lemonsu, A., Kounkou-Arnaud, R., Brion, D., Masson, V., 2020. Long time series spatialized data for urban climatological studies: A case study of Paris. France. Int. J. Climatol. 40, 3567–3584. https://doi.org/10.1002/joc.6414.

Lee, D.O., 1979. The influence of atmospheric stability and the urban heat island on urban-rural wind speed differences. Atmospheric Environ. 1967 (13), 1175–1180. https://doi.org/10.1016/0004-6981(79)90042-8.

Lehnert, M., Janků, Z., Novotný, D., Jurek, M., Geletič, J., 2025. Assessment of air temperature indices and urban heat island intensity based on two meteorological networks in Prague. Czechia. Theor. Appl. Climatol. 156, 470. https://doi.org/10.1007/s00704-025-05707-5.

Lemonsu, A., Caillaud, C., Alias, A., Riette, S., Seity, Y., Le Roy, B., Michau, Y., Lucas-Picher, P., 2023. What added value of CNRM-AROME convection-permitting regional climate model compared to CNRM-ALADIN regional climate model for urban climate studies ? Evaluation over Paris area (France). Clim. Dyn. 61, 1643–1661. https://doi.org/10.1007/s00382-022-06647-w.

Liu, J., Niyogi, D., 2019. Meta-analysis of urbanization impact on rainfall modification. Sci. Rep. 9, 7301. https://doi.org/10.1038/s41598-019-42494-2.

Lucas-Picher, P., Argüeso, D., Brisson, E., Tramblay, Y., Berg, P., Lemonsu, A., Kotlarski, S., Caillaud, C., 2021. Convection-permitting modeling with regional climate models: Latest developments and next steps. WIREs Clim. Change 12, e731. https://doi.org/10.1002/wcc.731.

Luo, M., Lau, N.-C., 2019. Urban Expansion and Drying Climate in an Urban Agglomeration of East China. Geophys. Res. Lett. 46, 6868–6877. https://doi.org/10.1029/2019GL082736.

Marquès, E., Messier, K.P., 2025. Improved high resolution heat exposure assessment with personal weather stations and spatiotemporal Bayesian models. GeoHealth 9. https://doi.org/10.1029/2025GH001451 e2025GH001451.

Masson, V., 2000. A Physically-Based Scheme For The Urban Energy Budget In Atmospheric Models. Bound.-Layer Meteorol. 94, 357–397. https://doi.org/10.1023/A:1002463829265.

Masson, V., Grimmond, C.S.B., Oke, T.R., 2002. Evaluation of the Town Energy Balance (TEB) Scheme with Direct Measurements from Dry Districts in Two Cities. J. Appl. Meteorol. Climatol. 41, 1011–1026. https://doi.org/10.1175/1520-0450(2002)041%3C1011:EOTTEB%3E2.0.CO;2.

Masson, V., Lemonsu, A., Hidalgo, J., Voogt, J., 2020. Urban Climates and Climate Change. Annu. Rev. Environ. Resour. 45, 411–444. https://doi.org/10.1146/annurev-environ-012320-083623.

Maucha, G., Büttner, G., Kosztra, B., 2010. EuropeanValidation of GMES FTS Soil Sealing Enhancement Data; Final draft. Copenhagen, Denmark, European Environment Agency.

Maurer, V., Düsterhöft-Wriggers, W., Beddig, R., Meyer, J., Hinrichs, C., Ho-Hagemann, H.T.M., Staneva, J., Ehlers, B.-M., Janssen, F., 2026. Evaluation of coupled and uncoupled ocean–ice–atmosphere simulations using icon-2024.07 and NEMOv4.2.0 for the EURO-CORDEX domain. Geosci. Model Dev. 19, 543–578. https://doi.org/10.5194/gmd-19-543-2026.

Meili, N., Paschalis, A., Manoli, G., Fatichi, S., 2022. Diurnal and seasonal patterns of global urban dry islands. Environ. Res. Lett. 17, 054044. https://doi.org/10.1088/1748-9326/ac68f8.

Melchiorri, M., Mari Rivero, I., Florio, P., Schiavina, M., Krasnodebska, K., Politis, P., Uhl, J., Pesaresi, M., Maffenini, L., Sulis, P., Crippa, M., Guizzardi, D., Pisoni, E., Belis, C., Oom, D., Branco, A., Mwaniki, D., Githira, D., Kochulem, E., Tommasi, P., Carioli, A., Ehrlich, D., Kemper, T., Dijkstra, L., 2024. Stats in the city: the GHSL urban centre database 2025 : public release GHS UCDB R2024. Publications Office of the European Union.

Menne, M.J., Durre, I., Vose, R.S., Gleason, B.E., Houston, T.G., 2012. An Overview of the Global Historical Climatology Network-Daily Database. J. Atmospheric Ocean. Technol. 29, 897–910. https://doi.org/10.1175/JTECH-D-11-00103.1.

Michau, Y., Lemonsu, A., Lucas-Picher, P., Caillaud, C., 2022. Evaluation of the Urban Heat Island of 12 Cities of France in a High-Resolution Regional Climate Model Simulation. https://doi.org/10.2139/ssrn.4213505.

Michau, Y., Lemonsu, A., Lucas-Picher, P., Bastin, S., Caillaud, C., de Vries, H., Adinolfi, M., Raffa, M., Katragkou, E., Coppola, E., 2025. Projected evolution of the Urban climate and heatwaves using an ensemble of convection-permitting regional climate models. Clim. Change 178, 154. https://doi.org/10.1007/s10584-025-03990-9.

Mikhailuta, S.V., Lezhenin, A.A., Pitt, A., Taseiko, O.V., 2017. Urban wind fields: Phenomena in transformation. Urban Clim. 19, 122–140. https://doi.org/10.1016/j.uclim.2016.12.005.

Nikulin, G., Buntemeyer, L., Fernández, J., McGinnis, S., Evans, J.P., 2025. CORDEX-CMIP6 Archiving Specifications for Dynamical Downscaling. https://doi.org/10.5281/zenodo.15047096.

Nogueira, M., Soares, P.M.M., 2019. A surface modelling approach for attribution and disentanglement of the effects of global warming from urbanization in temperature extremes: application to Lisbon. Environ. Res. Lett. 14, 114023. https://doi.org/10.1088/1748-9326/ab465f.

Nogueira, M., Lima, D.C.A., Soares, P.M.M., 2020. An integrated approach to project the future urban climate response: Changes to Lisbon's urban heat island and temperature extremes. Urban Clim. 34, 100683. https://doi.org/10.1016/j.uclim.2020.100683.

Niu, Guo-Yue, Yang, Zong-Liang, Mitchell, Kenneth E., Chen, Fei, Ek Michael, B., Barlage, Michael, Kumar, Anil, Manning, Kevin, Niyogi, Dev, Rosero Enrique, Tewari Mukul, 2011. The community Noah land surface model with multiparameterization options (Noah-MP): 1. model description and evaluation with local-scale measurements. J. Geophys. Res. Space Phys. 116 (D12).

Nogueira, M., Hurduc, A., Ermida, S., Lima, D.C.A., Soares, P.M.M., Johannsen, F., Dutra, E., 2022. Assessment of the Paris urban heat island in ERA5 and offline SURFEX-TEB (v8.1) simulations using the METEOSAT land surface temperature product. Geosci. Model Dev. 15, 5949–5965. https://doi.org/10.5194/gmd-15-5949-2022.

Oke, T.R., Mills, G., Christen, A., Voogt, J.A., 2017. Urban Climates. Cambridge University Press, Cambridge. https://doi.org/10.1017/9781139016476.

Oleson, A.K.W., Lawrence, A.D.M., Bonan, A.G.B., Drewniak, A.B., Huang, A.M., Koven, A.C., Levis, A.S., Li, A.F., Riley, A.W., Subin, A.Z., Swenson, A.S., Thornton, A. P., Bozbiyik, A.A., Fisher, A.R.A., Heald, A.C., Kluzek, A.E., Lamarque, A.J.-F., Lawrence, A.P.J., Leung, A.L., Lipscomb, A.W., Muszala, A.S.P., Ricciuto, A.D., Sacks, A.W.J., Sun, A.Y., Tang, A.J., Yang, A.Z., 2013a. Technical description of version 4.5 of the Community Land Model (CLM).

Oleson, K., Lawrence, D., Bonan, G., Drewniak, B., Huang, M., Koven, C., Levis, S., Li, F., Riley, W., Subin, Z., Swenson, S., Thornton, P., Bozbiyik, A., Fisher, R., Heald, C., Kluzek, E., Lamarque, J.-F., Lawrence, P., Leung, L., Lipscomb, W., Muszala, S., Ricciuto, D., Sacks, W., Sun, Y., Tang, J., Yang, Z.-L., 2013b. Technical description of version 4.5 of the Community Land Model (CLM). [object Object]. https://doi.org/10.5065/D6RR1W7M.

Pedruzo-Bagazgoitia, X., Sützl, B., Dutra, E., McNorton, J., Tsiringakis, A., Rüdiger, C., 2026. Unlocking urban climate change analysis in global kilometer-scale climate simulations. Geophysical Research Letters 53. https://doi.org/10.1029/2025GL120583 e2025GL120583.

Peterson, T.C., 2003. Assessment of Urban Versus Rural In Situ Surface Temperatures in the Contiguous United States: No Difference Found. J. Clim. 16, 2941–2959. https://doi.org/10.1175/1520-0442(2003)016%3C2941:AOUVRI%3E2.0.CO;2.

Pietikäinen, J.-P., Freisen, P., Buntemeyer, L., Hoffmann, P., Jacob, D., Langendijk, G.S., Le Roy, B., Lemonsu, A., Masson, V., Pop, C., Rechid, D., Sieck, K., Ziegler, K, Teichmann, C., 2026. The REgional climate MOdel REMO2020-TEB: integration, development, and evaluation of the Town Energy Balance model. to be submitted to: Geoscientific Model Development, in preparation.

Pietikäinen, J.-P., Sieck, K., Buntemeyer, L., Frisius, T., Nam, C., Hoffmann, P., Pop, C., Rechid, D., Jacob, D., 2025. REMO2020: a modernised modular regional climate model. Geosci. Model Dev. 18, 7907–7949. https://doi.org/10.5194/gmd-18-7907-2025.

Pongracz, R., Bartholy, J., Lelovics, E., Dezső, Z., 2010. Comparison of the urban heat island effect calculated from ground-based and remotely sensed temperature observations.

Prein, A.F., Gobiet, A., Truhetz, H., Keuler, K., Goergen, K., Teichmann, C., Maule, C.F., Meijgaard, E. van, Déqué, M., Nikulin, G., Vautard, R., Colette, A., Kjellström, E., Jacob, D., 2015. Precipitation in the EURO-CORDEX 0.11^{\circ } and 0.44^{\circ } simulations: high resolution, high benefits? Clim. Dyn. 46, 383–412. doi: https://doi.org/10.1007/s00382-015-2589-y.

Rasul, A., Balzter, H., Smith, C., 2016. Diurnal and Seasonal Variation of Surface Urban Cool and Heat Islands in the Semi-Arid City of Erbil. Iraq. Climate 4, 42. https://doi.org/10.3390/cli4030042.

Rechid, D., Raddatz, T.J., Jacob, D., 2008. Parameterization of snow-free land surface albedo as a function of vegetation phenology based on MODIS data and applied in climate modelling. Theor Appl Clim. 95, 245–255. https://doi.org/10.1007/s00704-008-0003-y.

Rechid, D., Davin, E., de Noblet-Ducoudré, N., Katragkou, E., 2017. CORDEX Flagship Pilot Study "LUCAS - Land Use & Climate Across Scales" - a new initiative on coordinated regional land use change and climate experiments for Europe. Presented at the EGU General Assembly Conference Abstracts, p. 13172.

Dataset Record: ESA Land Cover Climate Change Initiative (Land_Cover_cci): Global Land Cover Maps, Version 1.6.1, n.d. URL https://catalogue.ceda.ac.uk/uuid/4761751d7c844e228ec2f5fe11b2e3b0/ (accessed 3.26.26).

Reinhart, V., Fonte, C.C., Hoffmann, P., Bechtel, B., Rechid, D., Boehner, J., 2021. Comparison of ESA climate change initiative land cover to CORINE land cover over Eastern Europe and the Baltic States from a regional climate modeling perspective. Int. J. Appl. Earth Obs. Geoinformation 94, 102221. https://doi.org/10.1016/j.jag.2020.102221.

Reinhart, V., Hoffmann, P., Rechid, D., Böhner, J., Bechtel, B., 2022. High-resolution land use and land cover dataset for regional climate modelling: a plant functional type map for Europe 2015. Earth Syst. Sci. Data 14, 1735–1794. https://doi.org/10.5194/essd-14-1735-2022.

Roth, M., Sanchez, B., Li, R., Velasco, E., 2022. Spatial and temporal characteristics of near-surface air temperature across local climate zones in a tropical city. Int. J. Climatol. 42, 9730–9752. https://doi.org/10.1002/joc.7862.

Russo, E., Geyer, B., Petrik, R., Keuler, K., Adinolfi, M., Feldmann, H., Goergen, K., Kerkweg, A., Kahin, P., Ludwig, P., Mertens, M., Pothapakula, P., Raffa, M., Rockel, B., Schulz, J.-P., Sulis, M., Hagemann, H., Truhetz, H., Uzan, I., Voggenberger, U., Steger, C., 2024. COSMO Technical Report No. 51 CLM Community WG EVAL, COordinated PArameter Testing project 2 (COPAT2): COSMO-CLM 6.0 clm1 recommended model configuration. https://doi.org/10.5676/DWD_PUB/NWV/COSMO-TR_51.

Schäfer, A.M., Ludwig, P., Krikau, S., Benz, S.A., Mühr, B., Mohr, S., Kunz, M., 2025. The evolution of heat exposure in changing societies and a changing climate from 1960 to 2100. Front. Clim. 7. https://doi.org/10.3389/fclim.2025.1491695.

Schär, C., Fuhrer, O., Arteaga, A., Ban, N., Charpilloz, C., Girolamo, S.D., Hentgen, L., Hoefler, T., Lapillonne, X., Leutwyler, D., Osterried, K., Panosetti, D., Rüdisühli, S., Schlemmer, L., Schulthess, T.C., Sprenger, M., Ubbiali, S., Wernli, H., 2020. Kilometer-Scale Climate Models: Prospects and Challenges. Bull. Am. Meteorol. Soc. 101, E567–E587. https://doi.org/10.1175/BAMS-D-18-0167.1.

Schlünzen, K.H., Hoffmann, P., Rosenhagen, G., Riecke, W., 2010. Long-term changes and regional differences in temperature and precipitation in the metropolitan area of Hamburg. Int. J. Climatol. 30, 1121–1136. https://doi.org/10.1002/joc.1968.

Schulz, J.-P., Vogel, G., 2020. Improving the Processes in the Land Surface Scheme TERRA: Bare Soil Evaporation and Skin Temperature. Atmosphere 11, 513. https://doi.org/10.3390/atmos11050513.

Schwingshackl, C., Daloz, A.S., Iles, C., Aunan, K., Sillmann, J., 2024. High-resolution projections of ambient heat for major European cities using different heat metrics. Nat. Hazards Earth Syst. Sci. 24, 331–354. https://doi.org/10.5194/nhess-24-331-2024.

Shepherd, J.M., 2006. Evidence of urban-induced precipitation variability in arid climate regimes. J. Arid Environ. 67, 607–628. https://doi.org/10.1016/j.jaridenv.2006.03.022.

Siu, L.W., Hart, M.A., 2013. Quantifying urban heat island intensity in Hong Kong SAR. China. Environ. Monit. Assess. 185, 4383–4398. https://doi.org/10.1007/s10661-012-2876-6.

Smid, M., Russo, S., Costa, A.C., Granell, C., Pebesma, E., 2019. Ranking European capitals by exposure to heat waves and cold waves. Urban Clim. 27, 388–402. https://doi.org/10.1016/j.uclim.2018.12.010.

Sobolowski, S., Somot, S., Fernandez, J., Evin, G., Brands, S., Maraun, D., Kotlarski, S., Jury, M., Benestad, R.E., Teichmann, C., Christensen, O.B., Bülow, K., Buonomo, E., Katragkou, E., Steger, C., Sørland, S., Nikulin, G., McSweeney, C., Dobler, A., Palmer, T., Wilcke, R., Boé, J., Brunner, L., Ribes, A., Qasmi, S., Nabat, P., Sevault, F., Oudar, T., 2025. GCM Selection and Ensemble Design: Best Practices and Recommendations from the EURO-CORDEX Community. Bull. Am. Meteorol. Soc. 106, E1834–E1850. https://doi.org/10.1175/BAMS-D-23-0189.1.

Stewart, I.D., Oke, T.R., 2012. Local Climate Zones for Urban Temperature Studies. Bull. Am. Meteorol. Soc. 93, 1879–1900. https://doi.org/10.1175/BAMS-D-11-00019.1.

Trusilova, K., Schubert, S., Wouters, H., Früh, B., Grossman-Clarke, S., Demuzere, M., Becker, P., 2016. The urban land use in the COSMO-CLM model: a comparison of three parameterizations for Berlin. Meteorol. Z. 231–244. https://doi.org/10.1127/metz/2015/0587.

Tucker, S.O., Kendon, E.J., Bellouin, N., Buonomo, E., Johnson, B., Murphy, J.M., 2022. Evaluation of a new 12 km regional perturbed parameter ensemble over Europe. Clim. Dyn. 58, 879–903. https://doi.org/10.1007/s00382-021-05941-3.

UN-Habitat, 2015. Guiding Principles for City Climate Action Planning | UN-Habitat. URL. https://unhabitat.org/guiding-principles-for-city-climate-action-planning (accessed 1.26.26).

Venter, Z.S., Brousse, O., Esau, I., Meier, F., 2020. Hyperlocal mapping of urban air temperature using remote sensing and crowdsourced weather data. Remote Sens. Environ. 242, 111791. https://doi.org/10.1016/j.rse.2020.111791.

Voogt, J.A., Oke, T.R., 2003. Thermal remote sensing of urban climates. Remote Sens. Environ. 86, 370–384.

Wilby, R.L., 2003. Past and projected trends in London's urban heat island. Weather 58, 251–260. https://doi.org/10.1256/wea.183.02.

Wilhelm, C., Rechid, D., Jacob, D., 2014. Interactive coupling of regional atmosphere with biosphere in the new generation regional climate system model REMO-iMOVE. Geosci. Model Dev. 7, 1093–1114. https://doi.org/10.5194/gmd-7-1093-2014.

WMO, 2023. Guidance on Measuring, Modelling and Monitoring the Canopy Layer Urban Heat Island (CL-UHI) [WWW Document]. URL. https://library.wmo.int/records/item/58410-guidance-on-measuring-modelling-and-monitoring-the-canopy-layer-urban-heat-island-cl-uhi#.ZBzXA3bMI2x (accessed 3.25.26).

World Bank. [WWW Document], n.d. World Bank Open Data. URL https://data.worldbank.org (accessed 2.3.26).

Wouters, H., Demuzere, M., Ridder, K.D., van Lipzig, N.P.M., 2015. The impact of impervious water-storage parametrization on urban climate modelling. Urban Clim. 11, 24–50. https://doi.org/10.1016/j.uclim.2014.11.005.

Wouters, H., Demuzere, M., Blahak, U., Fortuniak, K., Maiheu, B., Camps, J., Tielemans, D., van Lipzig, N.P.M., 2016. The efficient urban canopy dependency parametrization (SURY) v1.0 for atmospheric modelling: description and application with the COSMO-CLM model for a Belgian summer. Geosci. Model Dev. 9, 3027–3054. https://doi.org/10.5194/gmd-9-3027-2016.

Yang, X., Li, Y., Luo, Z., Chan, P.W., 2017. The urban cool island phenomenon in a high-rise high-density city and its mechanisms. Int. J. Climatol. 37, 890–904. https://doi.org/10.1002/joc.4747.

Zazulie, N., Nogherotto, R., Coppola, E., Diez-Sierra, J., Raffaele, F., Giuliani, G., Outten, S., 2026. Future projections of Climate Hazards in Urban and Rural Areas for European Cities Using Euro-CORDEX ensemble. https://doi.org/10.21203/rs.3.rs-8368518/v1.

Zhan, C., Xie, M., Lu, H., Liu, B., Wu, Z., Wang, T., Zhuang, B., Li, M., Li, S., 2023. Impacts of urbanization on air quality and the related health risks in a city with complex terrain. Atmospheric Chem. Phys. 23, 771–788. https://doi.org/10.5194/acp-23-771-2023.

Zhang, F., Cai, X., Thornes, J.E., 2014. Birmingham's air and surface urban heat islands associated with Lamb weather types and cloudless anticyclonic conditions. Prog. Phys. Geogr. Earth Environ. 38, 431–447. https://doi.org/10.1177/0309133314538725.

Zhao, L., Lee, X., Smith, R.B., Oleson, K., 2014. Strong contributions of local background climate to urban heat islands. Nature 511, 216–219. https://doi.org/10.1038/nature13462.

Zhao, L., Oleson, K., Bou-Zeid, E., Krayenhoff, E.S., Bray, A., Zhu, Q., Zheng, Z., Chen, C., Oppenheimer, M., 2021. Global multi-model projections of local urban climates. Nat. Clim. Change 11, 152–157. https://doi.org/10.1038/s41558-020-00958-8.